TOPICAL REVIEW

Slow light in fiber Bragg gratings and its applications

IOP Publishing Journal of Physics D: Applied Physics
J. Phys. D: Appl. Phys. **49** (2016) 463001 (19pp) doi:10.1088/0022-3727/49/46/463001

Topical Review

Slow light in fiber Bragg gratings and its applications

George Skolianos[1], Arushi Arora[1], Martin Bernier[2] and Michel Digonnet[1]

[1] Edward L Ginzton Laboratory, Stanford University, Stanford, CA 94305, USA
[2] Centre d'optique, photonique et laser (COPL), Université Laval, Québec, Canada G1V 0A6, Canada

E-mail: arushi15@stanford.edu

Received 24 April 2015, revised 18 July 2016
Accepted for publication 30 August 2016
Published 26 October 2016

Abstract

Slow-light fiber Bragg gratings (FBGs) belong to a class of gratings designed to exhibit one or more narrow resonances in their reflection and transmission spectra, produced either by introducing a π phase shift near the middle of the grating, or by increasing the index modulation so that the grating behaves like a Fabry–Perot interferometer. These resonances can have very narrow linewidths (<50 fm), resulting in low group velocities and high Q factors. Slow-light gratings are finding a growing number of applications in many areas of photonics, including nonlinear optics, optical switching, optical delay lines, and sensing. This paper reviews the principle of these gratings, in particular the more recent slow-light gratings relying on a strong index modulation. It discusses in particular the requirements for achieving large group delays and high sensitivities in sensors, and the fabrication and annealing techniques used to meet these requirements (high index modulation, low loss, index-profile apodization, and optimized length). Several applications are presented, including record-breaking FBGs that exhibit a group delay of 42 ns and Q-factor of ~30 million over a 12.5 mm length, robust acoustic sensors with pressure resolution of ~50 μPa $(\sqrt{\text{Hz}})^{-1}$ in the few-kHz, and a strain sensor capable of resolving as little as 30 femtostrain $(\sqrt{\text{Hz}})^{-1}$.

Keywords: slow light, fiber Bragg grating, FBG

(Some figures may appear in colour only in the online journal)

1. Introduction

A fiber Bragg grating (FBG) is a short length (a few mm to a few cm) of optical fiber along which the refractive index of the core region is periodically modulated on a sub-wavelength scale. Light launched into a grating is subject to a small Fresnel reflection each time it encounters a local region where the index either increases or decreases. In the vicinity of a particular wavelength known as the Bragg wavelength, these multiple incremental reflected fields add coherently in phase, leading to a strong reflection peak, and a corresponding dip in the grating's transmission spectrum. An FBG therefore acts primarily as a narrowband reflector that transmits nearly perfectly well outside of its reflection window. The width of the reflection peak is controlled by the length, index modulation amplitude, and period of the FBG. It typically ranges from under 0.1 nm in weak gratings [1] (peak-to-peak modulations of 5×10^{-5} or less [1]) to a few hundred nm in chirped gratings [2]. The peak reflectivity typically ranges from less than 10% in weak gratings [3] to close to 100% in strong gratings [4] (large index modulations, up to ~10^{-2} [5]).

Since their invention in 1978 [6], FBGs have been widely used in many applications ranging from filters in optical communication systems [7] to cavity mirrors in fiber lasers [8] and semiconductor lasers [9]. Because the Bragg wavelength depends on the index and period of the grating, both of which are influenced by a large number of external parameters, FBGs are also widely used as sensors for a host of parameters, in particular strain and temperature [10, 11].

When used as a notch filter in optical communication systems [6], an FBG must strongly reflect the band of frequencies lying within the bandwidth of its reflection peak, and transmit all frequencies outside the peak. One way to achieve a strong reflection peak is to increase the index modulation [12]. In uniform FBGs (index modulation constant along the length) this leads to the formation of pronounced narrow side-lobes resonances on both sides of the peak [12–14]. In the vicinity of one of these resonances, light travels multiple times through the grating before exiting at either port, and therefore it experiences a longer group delay than light away from a resonance. The FBG then supports structural slow light, and the resonances are referred to as slow-light resonances. The larger the index modulation is, the more pronounced these lobes are, and the larger the group delay, or the slower the light. These lobes, whose physical origin will be described further on, are undesirable in communication applications because they result in cross-coupling between adjacent channels [15, 16]. They are typically suppressed by properly apodizing the index-modulation profile of the FBG [12, 13, 17].

Conversely, these same narrow resonances can be quite useful in other areas of photonics, in particular for developing high-sensitivity sensors or high-Q optical cavities. These resonances act as quasi-delta functions that also spectrally shift when the grating is subjected to certain external perturbations (strain, temperature, pressure etc). Thus by interrogating the spectral position of a resonance with a probe laser at a frequency tuned to the steepest slope of such a narrow resonance, even minute perturbations can be sensed, leading to ultra-sensitive sensors [18]. Furthermore, structural slow light can be used to enhance certain optical nonlinear effects present in the fiber, which can lead to interesting applications such as optical switching [19, 20]. Similarly, these slow-light resonances also offer the opportunity to confine light in time and space and provide cavities with high Purcell factors. As such, they offer an interesting potential for producing low-threshold lasers [21] and optical frequency combs [22, 23] for example, and new test beds for cavity quantum electrodynamics (CQED) experiments [24].

As a result of these interesting new applications, there has been recently an increased interest in understanding how to generate very sharp resonances in fiber Bragg gratings. Significant breakthroughs have been reported in specially designed FBGs of cm length scale, including resonances with a group delay as long as 42 ns and a Q as high as ~3×10^7 [25], and strain sensors with record-breaking sub-picostrain/$\sqrt{\text{Hz}}$ resolutions [18]. The primary objective of this article is to present a basic introduction to the techniques that have been developed to achieve exceptionally sharp slow-light resonances, to review and explain the principle of operation of some of these applications.

2. Background

2.1. Modeling FBGs

The modulated index profile of an FBG is illustrated in figure 1 in the common case of a uniform grating. It can be described mathematically for a more general index profile as [12]

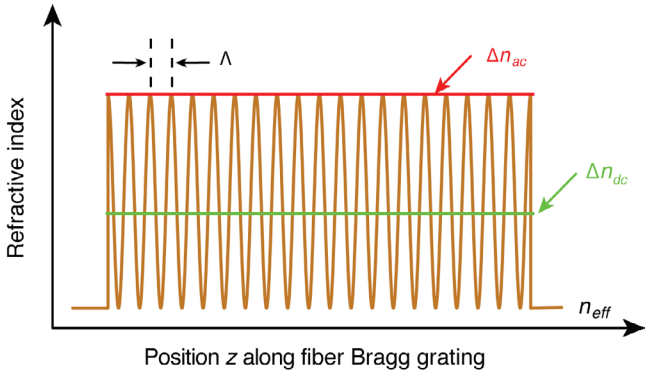

Figure 1. Periodically varying refractive index in a uniform FBG.

$$n(z) = n_{\text{eff}} + \Delta n_{\text{dc}}(z) + \Delta n_{\text{ac}}(z)\cos\left(\frac{2\pi z}{\Lambda} + \varphi(z)\right). \quad (1)$$

As defined in figure 1, n_{eff} is the initial effective refractive index of the fiber mode, Δn_{dc} is the mean change in refractive index, Δn_{ac} is half the peak-to-peak amplitude of the ac index modulation, Λ is the period of the grating, z is the position along the fiber, and $\varphi(z)$ is the additional phase modulation resulting from a possible chirp in the grating period. In a uniform grating, Δn_{dc} and Δn_{ac} have top-hat profiles that are independent of z within the grating and have abrupt edges at the ends of the grating (figure 1). In contrast, in an apodized grating the index profiles smoothly fall to zero at the edges of the grating.

When light is launched into an FBG, it is partially reflected each time it encounters a change of index, which occurs at every point along the rising and the falling edges of each period in the index modulation (see figure 1). These multiple delocalized reflections, of the order of thousands per mm, are coupled primarily to the backward fundamental mode of the fiber. The phase difference between reflections from any two adjacent peaks in the index modulation is $\Delta\phi = 2\pi\bar{n}2\Lambda/\lambda$, where λ is the wavelength of the light and $\bar{n}$ is the average index seen by the light as it traverses the FBG. At the Bragg wavelength $\lambda_{\text{B}} = 2\bar{n}\Lambda$, $\Delta\phi = 2\pi$, i.e. all these reflections add constructively, which results in a strong reflection peak. For a uniform grating, $\bar{n} = n_{\text{eff}} + \Delta n_{\text{dc}}$ (see equation (1)), which gives the conventional expression $\lambda_{\text{B}} = 2(n_{\text{eff}} + \Delta n_{\text{dc}})\Lambda$.

The forward (incident) and backward (reflected) propagating modes being coupled together, coupled-mode theory can be used to model the spectral characteristics of a grating, in particular the shape and magnitude of its reflection and transmission spectra [12]. For a uniform grating of length L, these coupled-mode equations can be solved analytically to obtain the power reflectivity spectrum r (modulus squared of the electric-field reflection coefficient spectrum ρ) of the grating [12, 26]:

$$r(\lambda) = |\rho|^2 = \frac{\sinh^2\left(\sqrt{\kappa^2 - \hat{\sigma}^2}L\right)}{\cosh^2\left(\sqrt{\kappa^2 - \hat{\sigma}^2}L\right) - \frac{\hat{\sigma}^2}{\kappa^2}}, \quad (2)$$

where the conventional ac coupling coefficient κ and the dc coupling coefficient σ are defined as

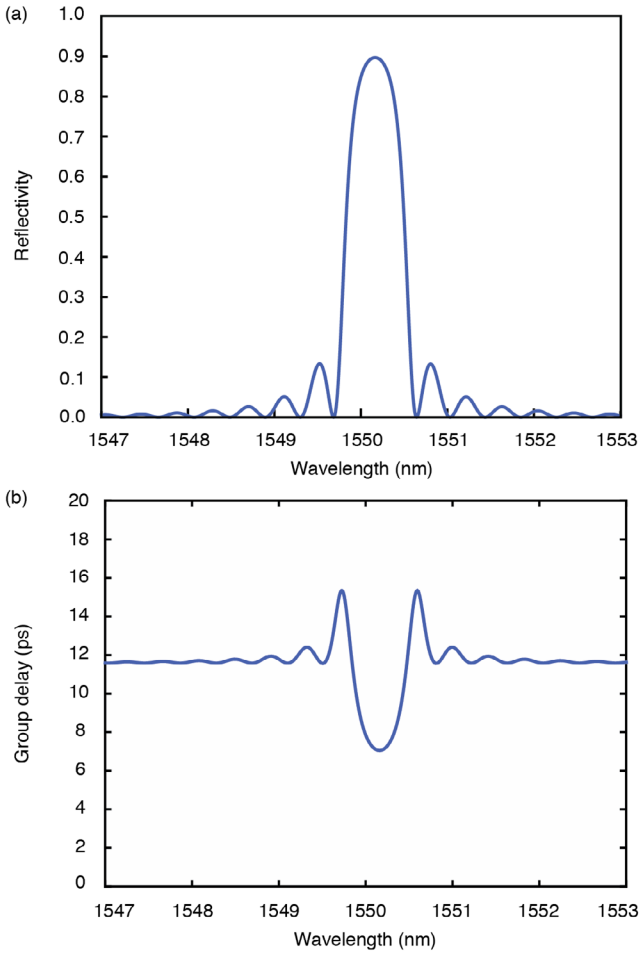

Figure 2. (a) Simulated reflection and (b) group delay spectra for a uniform FBG of length $L = 2$ mm, index modulation $\Delta n_{ac} = 4.4 \times 10^{-4}$ and period $\Lambda = 538.1$ nm.

$$\kappa = \pi \Delta n_{ac}/\lambda \tag{3}$$

$$\sigma = 2\pi \Delta n_{dc}/\lambda \tag{4}$$

and

$$\hat{\sigma} = \frac{2\pi n_{eff}}{\lambda} - \frac{\pi}{\Lambda} + \sigma. \tag{5}$$

The maximum reflectivity (at λ_B) is given by

$$r_{max} = \tanh^2(\kappa L) \tag{6}$$

Far away from the Bragg wavelength, the FBG acts as a normal fiber, i.e. it is essentially transparent. Figure 2(a) illustrates the reflection spectrum of a particular uniform grating, simulated using equation (2).

For a uniform grating, the bandwidth of the transmission (and reflection) peak, defined as the wavelength spacing between the first zeros on either side of the reflection peak maximum (see figure 2), depends on the ac index modulation Δn_{ac} and grating length L according to [12]

$$\Delta\lambda_B = \lambda_B \frac{\Delta n_{ac}}{n_{eff}} \sqrt{1 + \left(\frac{2n_{eff}\Lambda}{\Delta n_{ac} L}\right)^2}. \tag{7}$$

Being a multiple-wave interferometer, an FBG introduces dispersion in the reflected and transmitted light signals. If θ_ρ is the phase of the field reflection coefficient ρ, ω is the optical frequency, the group delay τ_g and group-delay dispersion d_ρ of the reflected light [12] are defined as

$$\tau_g = \frac{d\theta_\rho}{d\omega} = -\frac{\lambda^2}{2\pi c}\frac{d\theta_\rho}{d\lambda} = \frac{n_g L}{c} \tag{8}$$

$$d_\rho = \frac{d\tau_g}{d\lambda} = -\frac{2\pi c}{\lambda^2}\frac{d^2\theta_\rho}{d\omega^2} \tag{9}$$

where n_g is the group index and c is the speed of light in free space. Figure 2(b) illustrates the group delay spectrum calculated for the uniform grating whose reflectivity spectrum is shown in figure 2(a). The group delay is an important metric in the performance of optical delay lines as well as slow-light FBG devices with sharp resonances; in particular it contributes to the sensitivity and noise of strain sensors. It is proportional to the slope of the phase spectrum, which means that a high group delay is obtained by achieving a steep change in the phase of the transmission/reflection spectrum. The group-delay dispersion of FBGs can be quite large, especially in non-uniform FBGs. For example, an ~11 cm FBG designed with a gradually increasing coupling coefficient along its length had a measured dispersion d_p in transmission of ~2000 ps nm^{-1} over a ~0.1 nm bandwidth [27]. It was used to successfully compensate for group velocity dispersion acquired over ~100 km in a 10 Gb s^{-1} optical link. Chirped gratings are more effective dispersion compensators because they have larger stop bands and can thus be used at higher bit rates [28]. Two 40 cm chirped FBGs with large stop bands (~4 nm) were used in conjunction to demonstrate dispersion compensation for ~100 km of a 40 Gb s^{-1} optical link [29].

For non-uniform FBGs, the coupled-mode equations do not generally have a closed-form solution and must be solved numerically. In order to model non-uniform FBGs, a MATLAB® program was written to numerically calculate the transmission and group delay spectra based on the piecewise method described in [12]. The $\Delta n_{ac}(z)$, $\Delta n_{dc}(z)$ and the power loss coefficient $\gamma(z)$ that characterizes propagation in the grating are used as inputs in the program. The general shape of these functions is modeled after the beam profile used during fabrication of the grating. After the three desired profiles are obtained, the FBG is divided along its length into a small number N of uniform FBGs of equal length δL, approximately 100 [12]. The number of the uniform FBGs must be chosen so as to fulfill two requirements: (1) each uniform FBG must include several periods of the grating ($L \gg \Lambda$) in order for the analytical solution for the uniform FBG to be valid, and (2) the Δn_{ac}, Δn_{dc} and loss of the original FBG must not change significantly between the beginning and the end of any of the N uniform FBGs, otherwise this piecewise approximation breaks down.

For each uniform FBG, the transfer matrix that connects the forward (denoted with '+' superscript) and backward (denoted with '−' superscript) electric fields at its output and input at one particular wavelength λ is calculated. The output

of the ith uniform FBG is the input of the $(i+1)$th uniform FBG. Thus we can calculate the input electric field of the ith uniform FBG from the input of the $(i+1)$th uniform FBG [12]:

$$\begin{bmatrix} E_i^+ \\ E_i^- \end{bmatrix} = \begin{bmatrix} \cosh\left(\sqrt{\kappa_i^2-\sigma_i^2}\cdot\delta L\right) - \mathrm{i}\dfrac{\sigma_i^2}{\sqrt{\kappa_i^2-\sigma_i^2}}\sinh\left(\sqrt{\kappa_i^2-\sigma_i^2}\cdot\delta L\right) & -\mathrm{i}\dfrac{\kappa_i^2}{\sqrt{\kappa_i^2-\sigma_i^2}}\sinh\left(\sqrt{\kappa_i^2-\sigma_i^2}\,\delta L\right) \\ \mathrm{i}\dfrac{\kappa_i^2}{\sqrt{\kappa_i^2-\sigma_i^2}}\sinh\left(\sqrt{\kappa_i^2-\sigma_i^2}\,\delta L\right) & \cosh\left(\sqrt{\kappa_i^2-\sigma_i^2}\cdot\delta L\right) + \mathrm{i}\dfrac{\sigma_i^2}{\sqrt{\kappa_i^2-\sigma_i^2}}\sinh\left(\sqrt{\kappa_i^2-\sigma_i^2}\cdot\delta L\right) \end{bmatrix} \begin{bmatrix} E_{i+1}^+ \\ E_{i+1}^- \end{bmatrix} = A_i \begin{bmatrix} E_{i+1}^+ \\ E_{i+1}^- \end{bmatrix} \tag{10}$$

where κ_ι and σ_ι are the ac and dc coupling coefficients, respectively, for the ith uniform FBG given by:

$$\sigma_i = 2\pi(n_0 + \Delta n_{\mathrm{dc}}^i)\left(\frac{1}{\lambda} - \frac{1}{\lambda_{\mathrm{B}}}\right) - \mathrm{i}\frac{\gamma^i}{2} \tag{11a}$$

$$\kappa_i = \pi\frac{\Delta n_{\mathrm{ac}}^i}{\lambda}. \tag{11b}$$

Afterwards, by multiplying the transfer matrices for all the N segments, a single matrix C is obtained that relates the input and output electric fields of the whole FBG [12]:

$$\begin{bmatrix} E_{\mathrm{in}}^+ \\ E_{\mathrm{in}}^- \end{bmatrix} = \begin{bmatrix} E_1^+ \\ E_1^- \end{bmatrix} = A_1 A_2 \cdots A_N \begin{bmatrix} E_{\mathrm{out}}^+ \\ E_{\mathrm{out}}^- \end{bmatrix} = C \begin{bmatrix} E_{\mathrm{out}}^+ \\ E_{\mathrm{out}}^- \end{bmatrix}. \tag{12}$$

From equation (12) assuming no backward propagating ($E_{\mathrm{out}}^- = 0$) field is injected into the FBG (as is the case in sensing and other applications) the field transmission and reflection coefficient can be easily calculated by evaluating C numerically. Then it is trivial to calculate the reflection and group delay spectra.

2.2. Generating slow-light resonances in FBGs

As mentioned in the introduction, for a broad range of applications there has been a growing interest in FBGs that exhibit one or more narrow resonances. Over the years, several approaches have been developed to produce such gratings, namely weak periodic and aperiodic gratings, superstructure, π-shifted, tilted or strong uniform gratings, and more recently strong apodized gratings [14, 30–34].

A narrow reflection peak can be created in a nominally uniform grating if its ac index modulation is small ($\Delta n_{\mathrm{ac}} \ll 2n_{\mathrm{eff}}\Lambda/L$, see equation (7)). The linewidth of the reflection peak then decreases in inverse proportion to the FBG length. While this method requires a weak grating and can therefore be conveniently implemented with any FBG-writing techniques, the narrow peaks that it produces have a low reflectivity because of the low modulation. As a result, the index modulation can only be so low, and the linewidth so narrow, before the peak disappears. This method therefore cannot produce a reflection that is both strong (high reflectivity) and narrow in a short grating. For example, in [3] an FBG with a narrow reflection peak bandwidth of 0.05 nm was demonstrated, but its peak reflectivity was only ~10%. Gagné *et al* [35] demonstrated the fabrication of a 2.5 pm bandwidth grating with a peak reflectivity of 99.9%, but it was very long (1 m).

A π-shifted grating is a good method to generate a resonance that is both strong and narrow [7]. It consists of an FBG in which a π phase shift has been introduced during fabrication at or near the middle of it, as illustrated in the inset of figure 3. This type of grating can be more easily conceptualized as two nominally identical FBGs separated by a gap of length $\lambda/4$, which means that light traveling in the gap accumulates a phase of π per round trip. Each grating acts as a reflector, and the two gratings together form a Fabry–Perot (FP) interferometer. This FP is so short that it supports a single transmission resonance, located around the middle of the grating's usual reflection peak (see figure 3(a)) [7]. This resonance is narrow if the grating is long and/or strong enough, so that its reflectivity is large and the finesse of the FP high (see figure 3(b)). The resonance can also be strong provided, as in any FP, that the residual transmission of the 'output' reflector is matched to the internal loss of the grating.

A third method is the generation of narrow slow-light resonances on the edges of the bandgap of strong uniform gratings, as demonstrated through simulations in [12, 13] and experimentally in [36]. In an FBG, light in the vicinity of λ_{B} is strongly reflected, while light strongly detuned from λ_{B} is essentially fully transmitted. Light at intermediate wavelengths, i.e. near an edge of the reflection peak, is strongly but not fully reflected, which means that some of it is transmitted, as illustrated by the top green path in figure 4. As it traverses the FBG back toward the input end, by virtue of reciprocity the reflected light is again strongly reflected and partially transmitted at the input port (second green path in figure 4). The second reflected signal travels to the output end of the grating, where it is again partially transmitted (third green path), and so on and so forth. This device again behaves analogously to an FP interferometer [13, 37], in which light is reflected back and forth between two mirrors, creating a comb of resonances. At certain wavelengths the multiple transmissions add constructively at the output end of the grating, leading to the formation of a series of narrow reflection peaks outside the bandgap [13, 37]. Figures 5(a) and (b) illustrates this principle with the reflection and group delay spectra calculated for a strong uniform grating.

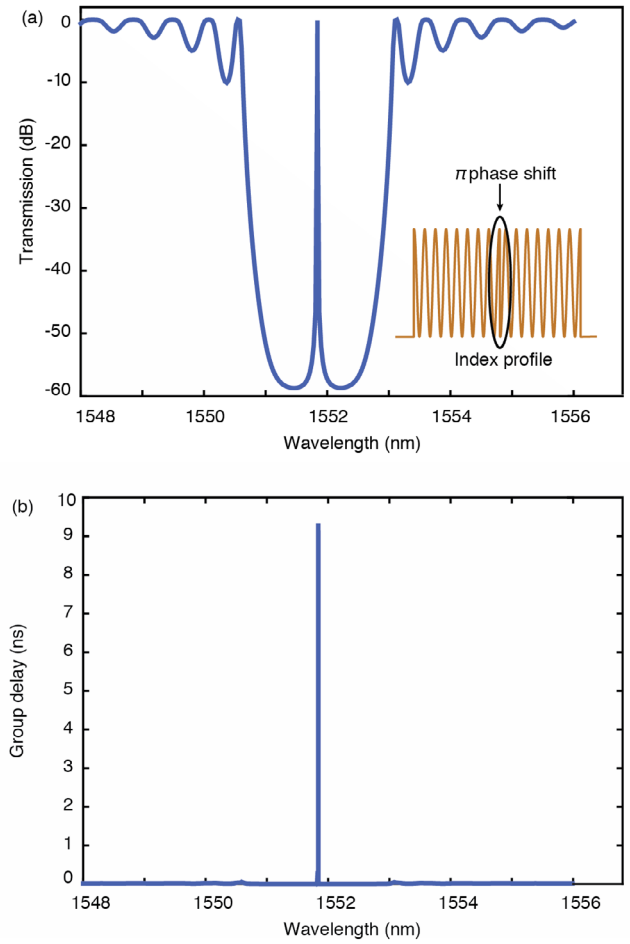

Figure 3. (a) Simulated transmission and (b) group delay spectra of a π-shifted FBG of length $L = 2\,\text{mm}$ with a uniform index modulation (shown in the inset) and an index modulation $\Delta n_{ac} = 2 \times 10^{-3}$, and a period $\Lambda = 538.1\,\text{nm}$.

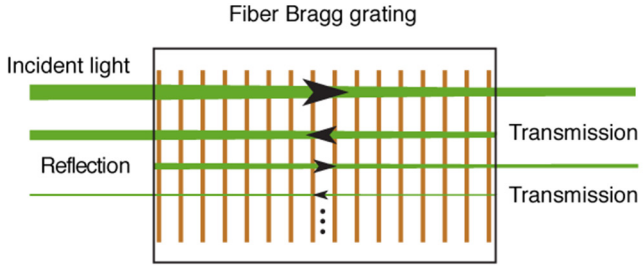

Figure 4. For wavelengths near the band-edge, multiple reflections from both ends of the FBG cause recirculation of light inside a strong FBG.

The spectrum now exhibits a series of narrow resonances on both sides of the bandgap. For the resonances to be narrow, the grating must have a strong enough index modulation to have a high reflectivity, and a low internal loss [38]. In addition, the resonances are strongest when the residual transmission of the FBG is matched to the internal loss, as in any FP [39]. These resonances are referred to as slow-light resonances because in their vicinity light travels back and forth along the FBG multiple times, and it consequently experiences an increased group delay, and a reduced apparent group velocity.

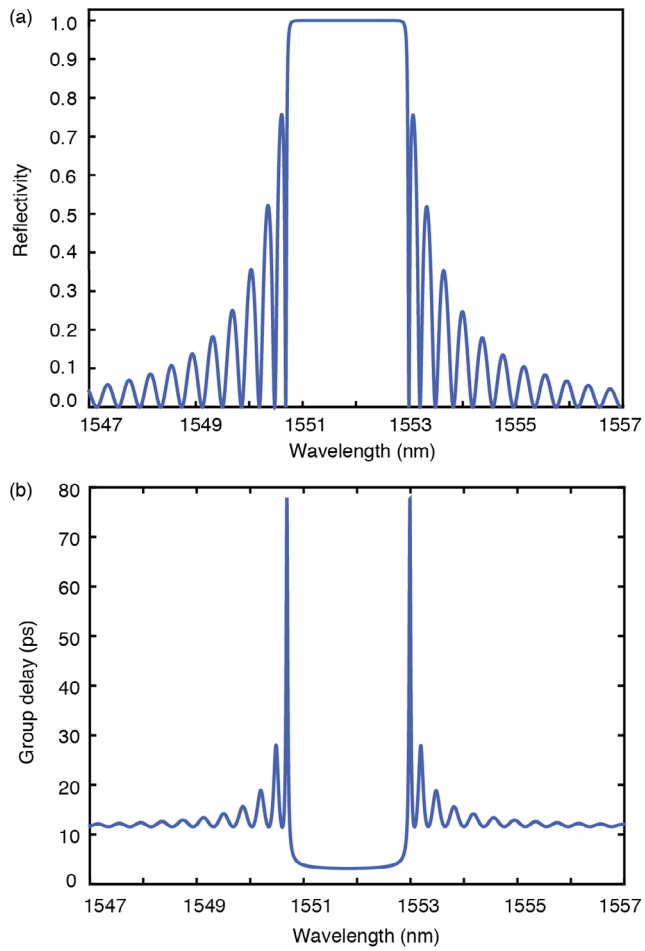

Figure 5. (a) Simulated reflection and (b) group delay spectra of a strong uniform grating showing strong slow-light resonances at both edges of the bandgap ($L = 2\,\text{mm}$, $\Delta n_{ac} = 2 \times 10^{-3}$, and $\Lambda = 538.1\,\text{nm}$).

Such resonances exist in conventional FBGs, i.e. FBGs with a weak (uniform or apodized) index modulation. However, they are very weak, with a group index barely larger than the phase index n_{eff} of the mode, and they offer none of the benefits of slow light discussed here. To clearly differentiate the two classes of gratings, in this manuscript 'slow-light FBG' refers strictly to a grating with at least one resonance that exhibits a group index many times ($\gtrsim$~10) larger than n_{eff}. As discussed further on, for many applications these slow-light resonances offer significant benefits over the weak resonances present in conventional FBGs, in general in proportion to their group index. This definition also applies to the next category of slow-light FBGs.

A fourth technique to create sharp resonances is a refined version of the third technique, namely a strong FBG with an apodized index profile. As illustrated in figure 6(a), the index profiles Δn_{ac} and Δn_{dc} are then functions of position, and so is the Bragg wavelength, according to

$$\lambda_B(z) = 2(n_{eff} + \Delta n_{dc}(z))\Lambda. \quad (13)$$

As a result of this spatial dependence, there are an infinite number of pairs of points along the FBG such that both points in the pair have the same Bragg wavelength. If the index profile is single-humped, as is often the case and as represented

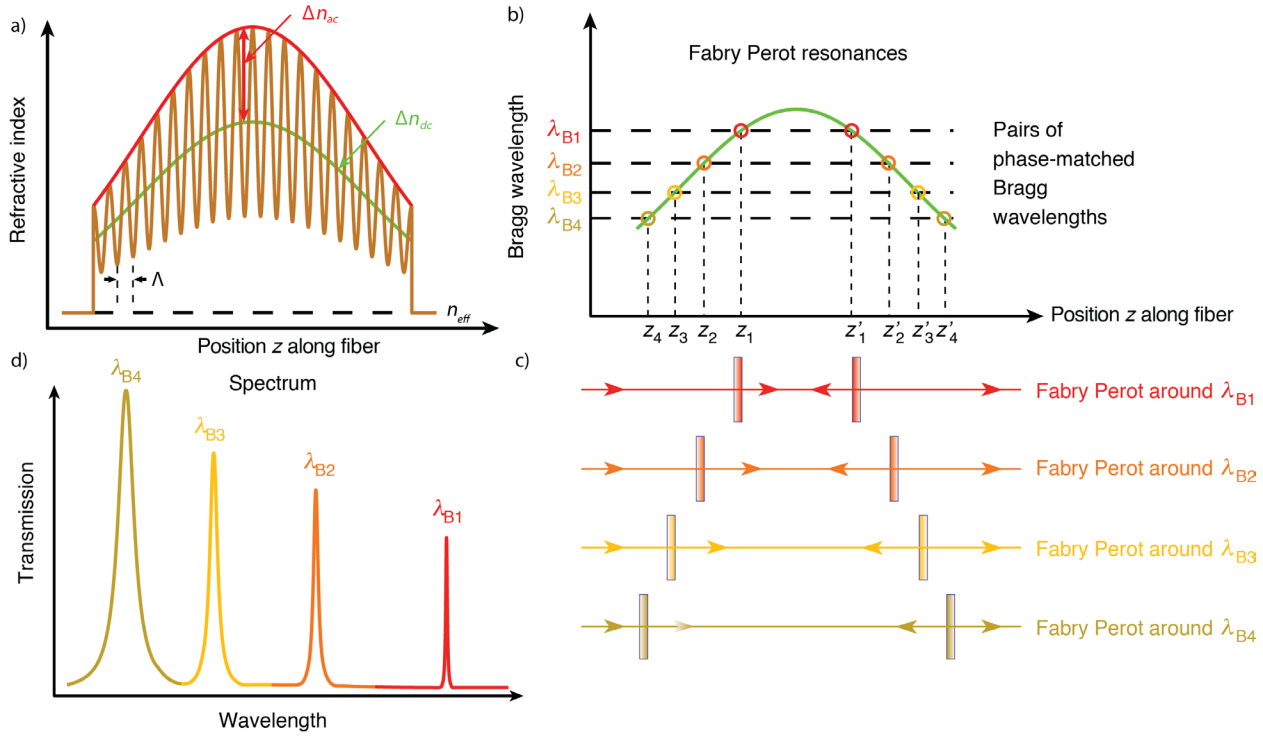

Figure 6. Apodized FBGs and slow light resonances through FPs. (a) The refractive index profile of an apodized FBG along its length (b) The distribution of Bragg wavelengths along FBG length (c) The Fabry-Perot resonances around each Bragg wavelength lead to (d) the emergence of slow light resonances in FBG transmission.

in figure 6(a), no two pairs have the same Bragg wavelength. A subset of four such pairs is shown in figure 6(b), located at (z_1, z_1'), (z_2, z_2'), (z_3, z_3'), and (z_4, z_4') and with respective Bragg wavelengths λ_{B1}, λ_{B2}, λ_{B3}, and λ_{B4}. Each pair acts as a pair of mirrors spaced by a distance $z_i - z_i'$ that reflect only in the vicinity of λ_{Bi}, and therefore form a Fabry–Perot interferometer around λ_{Bi}. Among this infinite set of FPs (z_i, z_i'), only a few have a spacing $z_i - z_i'$ such that light at λ_{Bi} is in phase with itself after a round-trip basis and the FP supports a resonance. The FBG then behaves like the superposition of these few resonant FPs (four are represented in the example of figure 6(c)). The mirror pair closest to the center of the FBG (z_1 and z_1' in figure 6(c)) has the largest Δn_{ac} of all mirrors, and therefore the highest reflectivity of all phase-matched pairs, and hence this FP supports the resonance with the highest Q factor. This mirror pair having also the shortest spacing, it supports the fundamental mode (the electric field distribution exhibits a single lobe along the FBG) [40, 41]. The other phase-matched pairs have a reflectivity that decreases with increasing distance from the center of the FBG [41, 42], and they support a broader resonance (figure 6(d)). Since they have a longer mirror spacing, they support a higher order mode (i.e. their electric field distributions have multiple lobes). A strong apodized FBG therefore exhibits a series of resonances narrower and generally stronger toward the center of the grating. An example of these slow-light resonances is provided in section 3.1.1.

A strong apodized FBG presents two key differences and advantages over a strong uniform FBG. From figure 6(b), it is clear that all points on the fiber lying between z_i and z_i' have Bragg wavelengths longer than λ_{Bi}; therefore the fiber between these two mirrors is transparent around λ_{Bi}. In contrast, in a uniform FBG the medium between the two mirrors is reflective at the Bragg wavelength, which leads to higher apparent internal loss. In addition, in an apodized FBG the resonances are formed just inside the bandgap instead of on the edge of the bandgap in a uniform FBG, and as a result the reflectivity of each mirror is higher. Thus, the resonances have a much higher Q factor than in a uniform FBG with similar characteristics [43].

Compared to π-shifted FBGs, apodized FBGs offer multiple resonances, each with different characteristics. These resonances can be useful individually (for sensing applications) or in combination with each other (for nonlinear applications where light at two or more wavelengths can interact resonantly in the same FBG).

2.3. Fabrication

An FBG is fabricated by modulating the refractive index of an optical fiber along its length at some period Λ, related to the target Bragg wavelength λ_B via equation (13). In that equation, the index modulation $\Delta n_{dc}(z)$ is generally weak compared to the unperturbed fiber index n_{eff}, and the period is approximately equal to $\lambda_B/(2n_{eff})$, or about a third of the Bragg wavelength for a silica fiber ($n_{eff} \approx 1.44$). A periodic index modulation is typically achieved by exposing the fiber to a writing laser beam that is modulated in amplitude either spatially or temporally. In the regions of the fiber exposed to light of suitable wavelength and intensity, the index of glass is increased, a phenomenon known as photosensitivity.

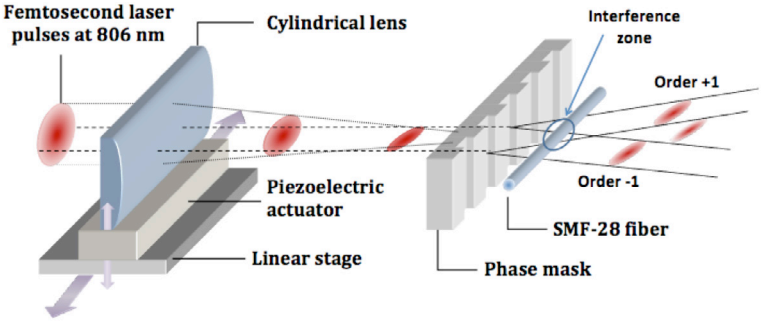

Figure 7. FBG fabrication setup using a movable femtosecond laser and a phase mask assembly.

Two main mechanisms have been identified to explain the photosensitivity of germanosilicate fibers [44]. The first one is formation of color centers induced by photo-excitation of precursors existing in the fiber. The most common precursors are oxygen deficiency defects Ge–Si and Ge–Ge, so-called wrong bonds (wrong in the sense that a Ge or Si atom is normally bonded to four oxygen atoms). When exposed to light of suitable wavelength and/or intensity, these wrong bonds strongly absorb and are broken, resulting in the formations of new species such as GeE', Ge(1) and Ge(2) [45]. These color centers exhibit strong absorption peaks in the UV and VUV [46]. The resulting change in the absorption spectrum of the fiber causes an increase in the index of the fiber according to the Kramers–Kronig relations [45].

The second mechanism is densification: the photon flux induces a local compaction of the glass matrix, which increases the refractive index proportionally to the increase in glass density [47]. The compaction also increases the tension in the fiber core, which slightly decreases the index due to the photoelastic effect [48]. In most fibers the measured net index change is positive. For a non-H_2-loaded fiber it was shown to be proportional to the induced stress [49].

The fiber can be loaded with hydrogen prior to exposure to enhance the photosensitivity. When exposed to the writing laser beam the presence of H_2 leads to the formation of GeH centers and to an increased efficiency in the formation of GeE' color centers [50]. Record index modulations in excess of 10^{-2} have been observed in H_2-loaded fibers [5]. However, it also increases the loss due to the introduction of broad absorption near 1.4 μm arising from OH^- radicals [51]. This can be mitigated by using deuterium instead of hydrogen, which also increases the photosensitivity but induces much lower loss around 1.5 μm since the absorption peak of OD^- radicals is around 1.9 μm [52].

The magnitudes of these two contributions (color centers and densification) are still the subject of much debate and interesting studies. They depend, sometime greatly, on the fabrication parameters, in particular the laser wavelength, laser intensity, and laser pulse width, as well as the fiber composition (glass type and possible presence of H_2/D_2) and its processing history.

Near-IR femtosecond lasers with ultra-high peak intensities (10^{12}–10^{13} W cm^{-2}) were recently reported to create gratings in H_2-loaded standard telecom fibers (Corning's SMF-28 fiber) through color-center formation with very large index modulations ($>5 \times 10^{-3}$) [2] and high thermal stability up to 350 °C [53]. The same technique was also reported to create gratings in non-H_2-loaded SMF-28 fibers via densification, with large index changes ($>2 \times 10^{-3}$) [54] and good thermal stability up to ~600–700 °C. This type of laser can also produce type-II damage gratings with tailored spectral responses sustaining temperatures above 1000 °C [55].

Femtosecond 800 nm Ti:sapphire amplifier systems have been used to fabricate gratings in all-silica, germanosilicate, and deuterium doped fibers using both phase-mask [54] and point-by-point [56] techniques [25, 54].

An apodized index profile [57] can be obtained using one of several techniques, including double exposure [58] and variable-diffraction-efficiency phase masks [17]. Longer FBGs can be inscribed through the scanning phase mask technique [59, 60], in which the laser beam (and the interference pattern) is slowly translated relative to the fiber, as illustrated in figure 7. These and other beneficial features of this apparatus have been reported in greater detail in [61, 62].

As in any resonator, it is important to minimize the internal loss of an FBG in order to obtain the strongest (narrowest) possible resonances [37, 38]. The internal loss of an FBG typically increases as the index modulation is increased [63]. For a given index modulation, FBGs written using near-IR femtosecond lasers have been shown to exhibit losses that are significantly lower than conventional UV-written FBGs [18, 40, 43, 62], by as much as a factor of approximately 4–5 [43]. For example, an FBG written in a conventional SMF-28 fiber had a measured Δn_{ac} of 0.99×10^{-3} and an inferred loss of only 0.1 m^{-1} [62]. Femtosecond lasers have consequently produced the slow-light FBGs with the highest group-delay and intensity enhancement performance so far.

The loss of an FBG can be reduced by thermal annealing, which involves heating the grating up to some maximum temperature, then letting it cool down to room temperature. The loss reduction results from a decay of defects and a rearrangement of the glass structure [64, 65]. For the same reasons, annealing also reduces the index modulation of the grating [64]. In slow-light femtosecond gratings, the first effect (loss reduction) increases the strength of the slow-light resonances (larger transmission, higher group index), while the second effect (index modulation reduction) does the opposite. The quantitative laws governing these effects are not known. In general, the temperature profile of the annealing process required to achieve a certain goal, for example to

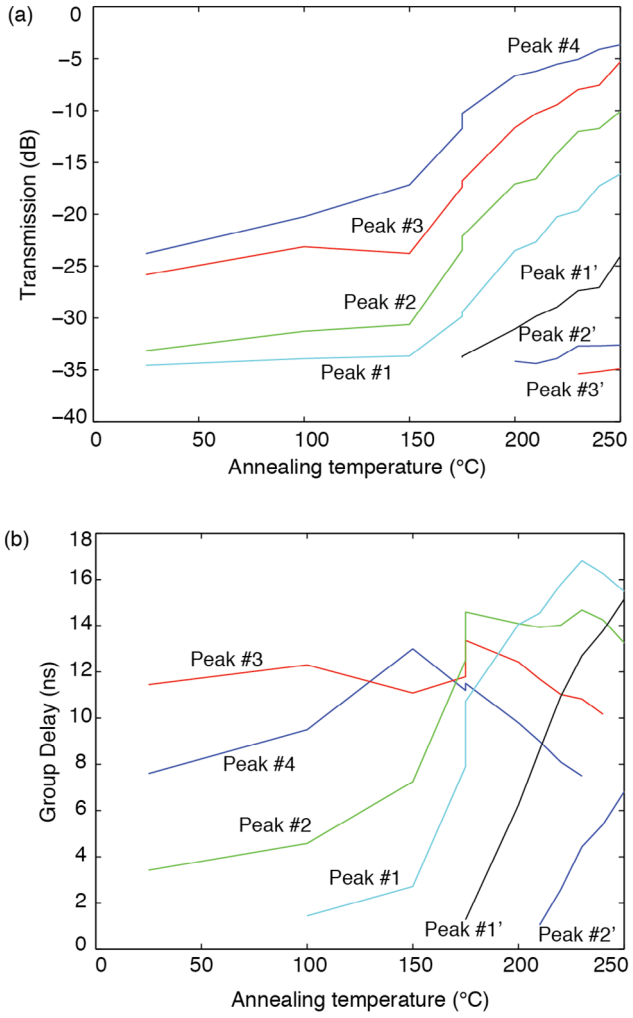

Figure 8. (a) Transmission evolution and (b) group delay evolution with annealing temperature measured in a femtosecond slow-light FBG.

maximize the group delay of any of the slow-light resonances, must therefore be determined empirically.

For example, consider a femtosecond grating [42] that exhibits four slow-light resonances prior to annealing, numbered in increasing number away from the bandgap as in figure 6(d). The measured peak transmission for these four resonances range monotonically from ~ − 35 dB to ~ −24 dB (see 25 °C data points in figure 8(a)). The measured group delays varied non-monotonically between ~3.5 and 11.5 ns (see figure 8(b)) (the group delay of peak #1 could not be measured because its power was too low). The grating was then annealed at a particular temperature in a fiber oven for 30 min. After the oven is switched off and the FBG has rapidly cooled down to room temperature, the transmission and group delay were re-measured. Their evolution with annealing temperature are shown in figures 8(a) and (b). Three important features have generally been observed [42]. First, for each peak the transmission increases monotonically with temperature, probably due to loss reduction. Second, new peaks appear inside the bandgap (labeled #1′, #2′, and #3′), because before annealing the loss was too high for them to have a measurable transmission. The transmissions of these new peaks also grow monotonically upon further annealing. Third, the group delay of a given resonance reaches a maximum at an optimum annealing temperature. This suggests that the effect of loss reduction dominates over the effect of the index modulation reduction up to an optimum temperature, and that at higher temperatures the trend is reversed. Figure 8 also shows that the deeper a resonance is into the bandgap, the higher its optimum temperature. Annealing is therefore a useful practical method to obtain high-transmission and high-group-delay resonances. To prevent having to strip the coating off the fiber before annealing, gratings can be made in fibers with polyimide jackets [61], a polymer that can withstand higher temperatures (~400 °C for short periods) than conventional fiber-jacket materials. This ensures the mechanical strength of the grating is not compromised because of annealing.

3. Applications

3.1. Communications

Slow-light FBGs can be used in optical communications as optical delay lines [25, 43] and as ultra-narrowband filters. They can also be useful components in all-optical signal processing [66] and for pulse shaping [67]. The presence of slow light by itself is a delay line, since the group delay is the time delay that a pulse experiences when it passes through a peak.

3.1.1. Delay lines. This section illustrates the substantial group delays that can be accomplished using slow-light FBGs. The full potential of these gratings for the generation of slow light was not exploited until relatively recently. The first significant breakthrough was a group index of ~5 in 2006, measured in a long (10 cm) apodized grating with a modest Δn_{ac} of 1.53×10^{-4} [68], corresponding to a group delay of ~1.7 ns. A much larger group index was made possible, as predicted in [12], by using a substantially stronger index modulation (~1.1×10^{-3}) in a slightly apodized grating with a nearly optimized length (1.2 cm) and probably a lower loss as well (1 m^{-1}). The slowest peak on the band edge of this grating had a measured group index of 130 [37], or a group delay of 5.2 ns. This result was confirmed in [40] with the publication of a comparable value in a strong, Gaussian-apodized grating.

Significantly greater group delays and concomitantly lower group velocities were achieved by making use of femtosecond FBGs because of their even stronger index modulations and lower internal loss. These strong apodized gratings were fabricated in an SMF-28 fiber with an 806 nm femtosecond laser using the scanning phase-mask technique. One such grating had a length of 2 cm, a Δn_{ac} of 1.69×10^{-3}, and a loss of 0.12 m^{-1}, and it delayed light by 20 ns [43].

This value has been recently doubled by bringing in two significant improvements, namely writing the grating in a deuterium-loaded fiber to increase the index modulation, and annealing the grating to reduce its loss [25]. The 12.5 mm FBG was annealed at 100 °C, 150 °C, 200 °C and then in steps of 10 °C and the group delay was monitored after each annealing step. At 370 °C, the peak third closest to the center

of the bandgap reached a maximum group delay of 42 ns, the current world record. The transmission and group-delay spectra of the grating measured at the end of this processing are plotted in figure 9 [25]. As predicted from physical principles (see figure 6(d)), the FBG exhibits several slow-light peaks on the short-wavelength edge of these two spectra, each corresponding to the resonance of an equivalent FP. The transmission peaks decrease in magnitude toward the center of the bandgap (see figure 9(a)), because light travels back and forth through the FBG more times and therefore suffers more loss. These peaks also become increasingly narrower as a result of greater reflectivity. The group-delay resonances (see figure 9(b)) grow correspondingly taller (larger group delays) toward the center of the bandgap, then decrease as a result of excessive loss. The slowest resonance (at ~1549.72 nm) had a group delay of 42 ns and a linewidth under 50 fm. It corresponds to a group velocity of only 300 km s^{-1}, a group index of 1010, the best values reported to date in an FBG.

It is clear that these very low group velocities are achieved at the cost of a limited bandwidth (50 fm in this case), which means in particular that as a group delay line such a device would function only with signals modulated at relatively low frequency. For devices such as these with a Lorentzian or Lorentzian-like lineshape, a steep slope implies a larger group index, but also a narrower bandwidth. In slow-light FBGs as in many other physical systems, the slow-light bandwidth is typically inversely proportional to the maximum group delay. Although it is possible to increase the bandwidth–group index product (for example by coupling optical resonators together), in general these approaches do not improve this product by orders of magnitude. There is almost always a relatively strict tradeoff between group delay and bandwidth.

3.1.2. Pulse shaping. Large group delays and high dispersions allow slow-light gratings to be used for pulse shaping [67]. The Fourier transform of the temporal impulse response is the reflectivity spectrum. For a weak grating the Fourier transform of the index profile is also proportional to the reflectivity spectrum. Thus, the index profile of a weak grating and the reflected pulse have the same shape. In [67], a π-shifted FBG was designed to shape an incident train of Gaussian pulses into a train of antisymmetric Hermite–Gaussian pulses. The π phase shift allowed the grating's index profile to be shaped as a Hermite–Gaussian (see figure 10). An inverse scattering method was used to design the peak-to-peak amplitude and length of the profile so that the FBG had the desired spectral response. The large apodization and combined with the π-shift gives the required spectral response to perform the transformation.

The FBG was written with a CW argon–ion laser using a scanning phase mask technique in which the fiber and phase mask were translated relative to the laser. A computer program dithered the translation stage to implement the desired apodization in the profile. The measured intensity profile of an individual Gaussian pulse launched in the FBG is shown in figure 11. The pulse train was reflected and filtered by the FBG, then collected using an circulator. The measured intensity of reflected pulse (see figure 11) shows that indeed the Gaussian pulse was shaped into an Hermite–Gaussian pulse.

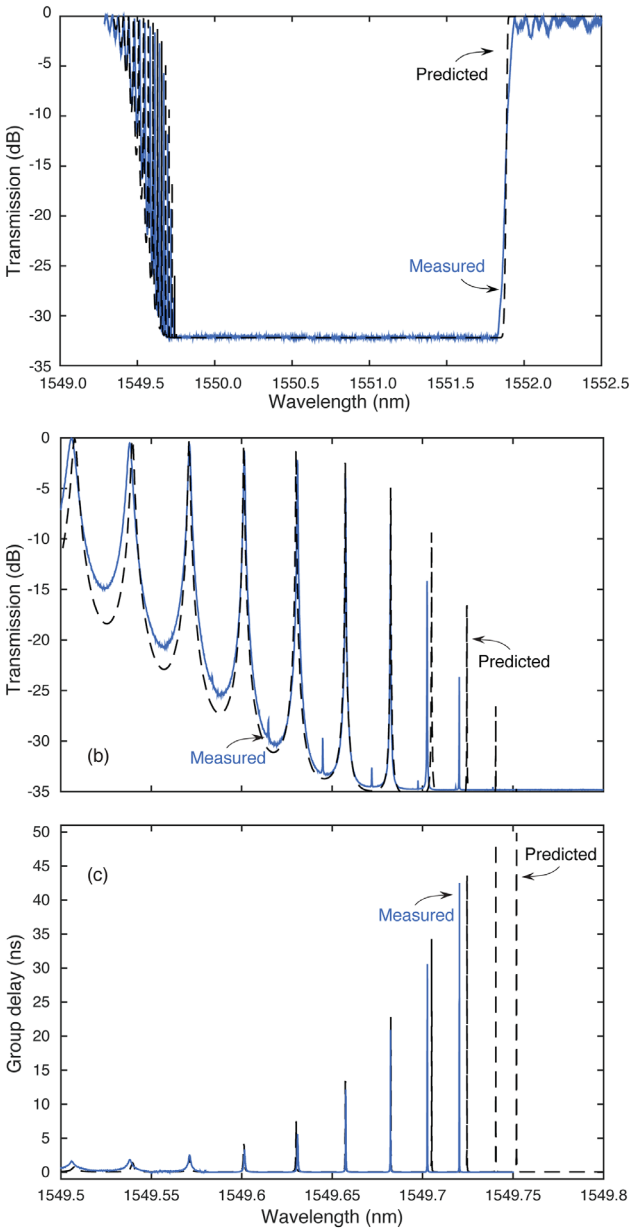

Figure 9. (a) Measured and simulated transmission spectra of the FBG. (b) Magnified portion of slow-light peak region of the transmission spectra shown in (a). (c) Measured and simulated group-delay spectra in the same wavelength range as in (b) (reproduced with permission from [25] The Optical Society, Copyright 2015).

When propagated through an 82 km length of single-mode fiber, the antisymmetric Hermite–Gauss pulses were broadened due to dispersion but they maintained their shape (see figure 11), which confirmed the antisymmetry of the pulses (π phase shift between the pulses' two peaks).

3.1.3. Signal processing. The steep slope in the phase change introduced in the light transmitted by a π-shifted grating can also be used to perform interesting all-optical information processing, such as calculating the temporal derivative of an optical signal [66]. The operating principle is the same as before: the slow-light FBG acts as a filter with

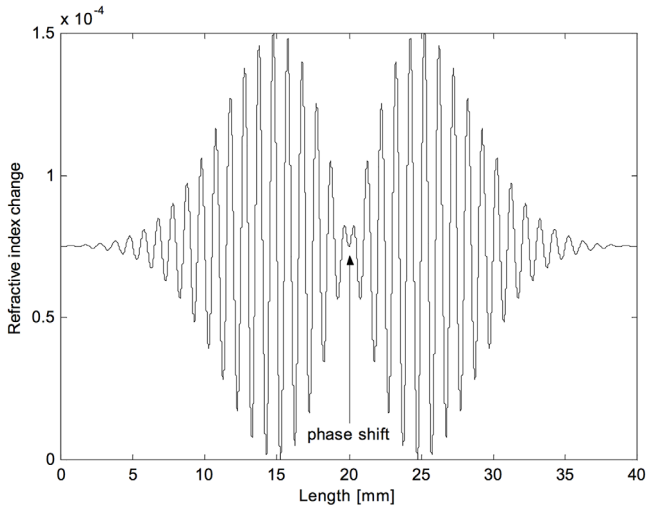

Figure 10. Simulated index profile for the π-shifted FBG used for pulse shaping (period of the grating is not to scale); reproduced with permission from [67] SPIE, Copyright 2001.

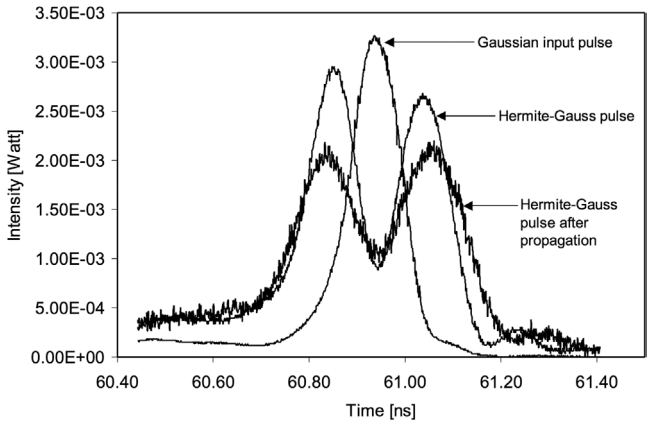

Figure 11. Experimental results of pulse shaping reproduced with permission from [67] SPIE, Copyright 2001. A custom π-shifted FBG of adequate dispersion is used to convert (shape) an input Gaussian pulse into a Hermite–Gaussian pulse. Also shown is the same pulse after propagating through an 82 km fiber.

a specific spectral response. In [66], a π-shifted FBG was fabricated in a hydrogen-loaded fiber using the phase-mask technique. The measured amplitude and phase of the FBG reflection spectrum are reproduced in the insets of figure 12 (only the aforementioned transmission resonance within the reflection peak is shown; the reflection peak itself is much broader than the range of wavelengths displayed in the insets). In the vicinity of this narrow slow-light transmission peak (see upper inset), the phase dependence on wavelength is almost linear and has a π jump (lower inset). When a signal at or near the resonance frequency travels through such a grating, its complex electric field is multiplied by $j\omega$, a transform that is equivalent to taking the derivative of the pulse temporal train. The measured input and output signals along with simulated results are plotted in figure 12. The output signal (figure 12(b)) resembles the derivative of the input signal (figure 12(a)), as expected. A π-shifted FBG can be used as a filter to perform other mathematical operations, such as the Hilbert transform [69].

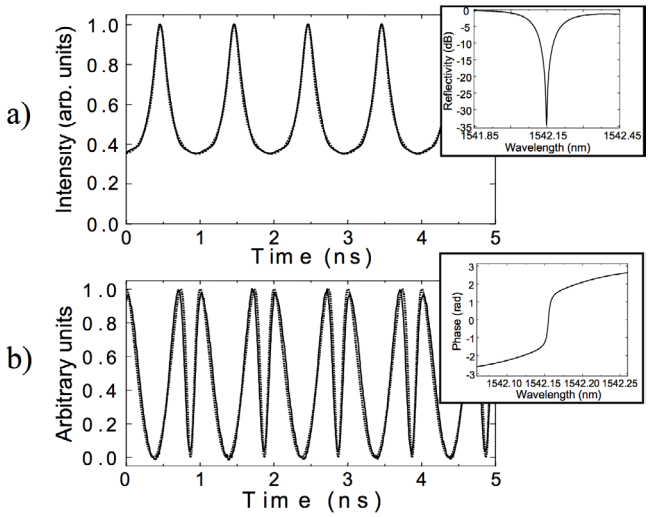

Figure 12. A π-shifted FBG was used to calculate the temporal derivative (trace (b)) of an input signal (trace (a)) © [2006] IEEE. Reprinted, with permission, from [66]. Solid lines: simulated results; dotted lines: experimental results. Insets: the measured amplitude and phase of the FBG's reflection spectrum.

Slow-light FBGs can also be used to create a single-sideband with carrier suppression for optical signals in radio-over-fiber applications. In [70], a simulated optical dual-sideband signal was transmitted through a π-shifted FBG. The laser signal wavelength was centered at 1547.8 nm with 0 dBm power. Initially, the optical power was amplitude modulated using an RF signal at 60 GHz at a bit rate of 500 Mbps. The two sidebands and the carrier are shown in figure 13(a). The initial power ratio between the carrier and the sidebands was 33.95 dB. This modulated signal was then filtered by passing it through a π-shifted FBG. The spectrum of the filtered signal transmitted by the FBG is shown in figure 13(b). The carrier has been greatly reduced, down to the level of the left sideband. The level of the right sideband was also reduced to ~21 dB below the left sideband. Thus, this signal can now propagate through the fiber with a much lower average power than the initial signal, which reduces undesirable nonlinear effects such as stimulated Brillouin scattering. Then, by using a fast photodetector the RF wave can be reproduced.

3.2. Nonlinear/QED applications

In section 3.1 we have shown that high group delays can be achieved in a properly designed FBG. A large group delay enhances certain nonlinear effects such as cross-phase modulation (XPM) and self-phase modulation (SPM), which can be used for interesting applications such as optical switching [19, 20]. Additionally, because FBGs exhibit a low group velocity in a short length (as short as a few mm), they can also offer high Purcell factors. Optical cavities with a high Purcell factor couple light efficiently to quantum emitters, and as such they also have interesting applications in low-threshold lasers [21], in cavity quantum electrodynamics (CQED) experiments [24], and to produce enhanced nonlinear interactions [71]. Examples of slow-light FBGs developed towards some of these applications are reviewed in this section.

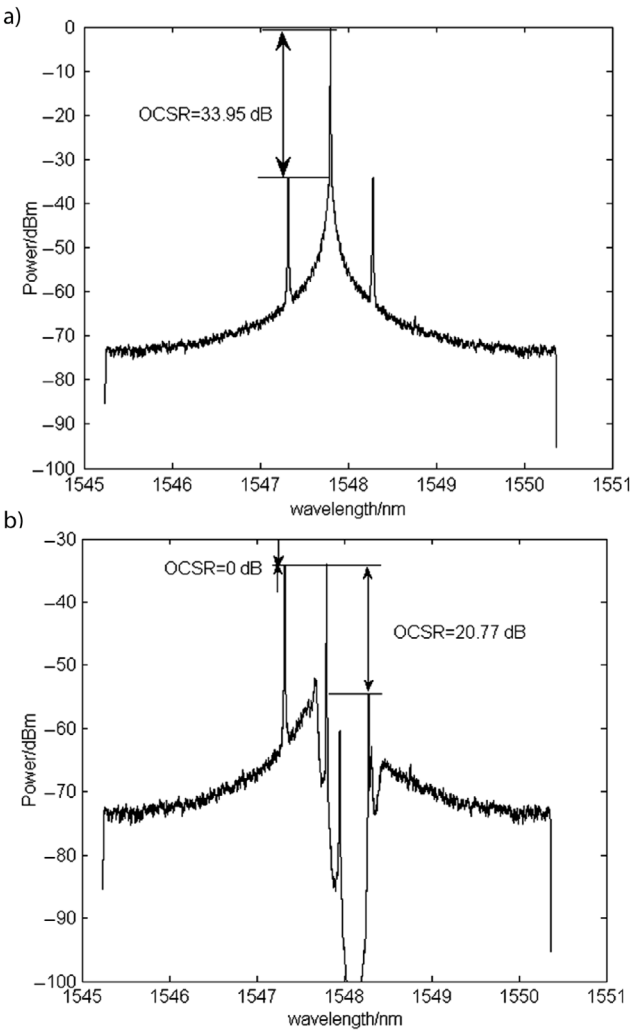

Figure 13. (a) Simulated spectrum of an RF-modulated optical signal. (b) Simulated spectrum after the signal has passed through a π-shifted FBG. Reprinted with permission from [70] SPIE, copyright 2013.

3.2.1. Nonlinear all-optical switches. Both XPM and SPM have their origins in the Kerr effect, a third-order nonlinear process by which the refractive index of the fiber material depends on the intensity of light. The change in refractive index due to intensity is given by equation (14) [72]:

$$\Delta n_{\mathrm{SPM,XPM}}(z,t) = n_2 I(z,t) \tag{14}$$

where n_2 is the third-order nonlinear index of the fiber and $I(z,t)$ is the light intensity. As a result, the phase of a signal traveling in a Kerr medium depends on its own intensity (SPM), and on the intensity of other signals (XPM).

Slow-light gratings utilizing the XPM effect can be used to make optical switches. A high intensity pump and a low power probe laser tuned to the peak of a slow-light resonance are launched into the grating. In the absence of the pump, the power of the probe signal detected at the output of the FBG is high and the switch is in its 'on' state. When a pump pulse is launched, a nonlinear index change is induced in the FBG due to XPM and the slow-light resonance shifts in the wavelength space. The probe signal is thus detuned from the slow-light peak, which causes a decrease in its output power. The switch is now in its 'off' state.

This effect is particularly attractive when implemented in a slow-light grating because the probe being tuned near a resonance, it recirculates many times in the grating, and the XPM that it experiences is enhanced in proportion to the number of recirculations. As a result, the pump power required to switch is reduced. An all-optical switch that uses this enhanced XPM effect was demonstrated in a π-shifted FBG operating at 1.55 μm [20]. The FBG was 20 mm long with a Gaussian-apodized index profile. The resonance had a measured FWHM bandwidth of 450 MHz and a measured peak transmission of 89%. The probe laser interrogated the FBG resonance at 1549.94 nm and a 1064 nm laser provided pump pulses to actuate the switching. After fitting the FBG spectrum to a model, the group index of the resonance was found to be ~5, which is approximately equal to the number of passes the probe made through the grating. The recirculation was therefore expected to lower the XPM pump-power requirement by a factor of ~5, as was indeed observed [20]. The resulting switch exhibited an extinction ratio of ~6 dB for a 1 kW pulse power. In this kind of a switch, there is a trade-off between speed and switching power. For the switch to operate at low power, a high group index is required (to have a large XPM enhancement), which means that the probe spends more time traveling back and forth through the device, and hence has a slower response time.

Slow-light gratings have also been used as optical switches by utilizing SPM instead of XPM. SPM can be observed if the intensity of the probe propagating in the FBG is large enough to cause a discernible nonlinear index change. This can be accomplished in two ways: (1) the input probe intensity is high, or (2) the input probe intensity is low but recirculation inside the FBG increases the internal intensity enough that SPM can be observed.

In [19], the intensity enhancement in a 2 mm π-shifted FBG was exploited to create such a switch. The input probe power controlled the position of the resonance and subsequently the transmission of the FBG at the probe wavelength. A numerical fit of the grating's measured transmission spectrum was used to calculate the ac coupling coefficient of the grating (from equation (3)), from which an expected intensity enhancement of 45 and an expected spectral shift of resonance of ~15 pm at an input power of 1 kW were calculated. In figure 14(a), the measured transmission spectrum of that FBG is shown for two different input powers. When the probe power was high (1 kW) the peak shifted toward longer wavelengths from its position at the lower power (~0.2 kW). This shift was measured to be 12 pm (see figure 14(b)), in general agreement with the expected value. The transmission of this FBG versus the input power is plotted in figure 15. Below a certain threshold power the probe wavelength is off resonance and the transmission is low ('off' state). When the input power was increased above this threshold, the resonance shifts to the probe wavelength and the transmission becomes large ('on' state). At threshold, the switch can be either in the 'on' or 'off' state depending on the previous state of the switch. The extinction ratio of the switch was used to experimentally verify the predicted intensity enhancement of 45. This enhanced Kerr effect was also used for shaping pulses propagating through an FBG [19].

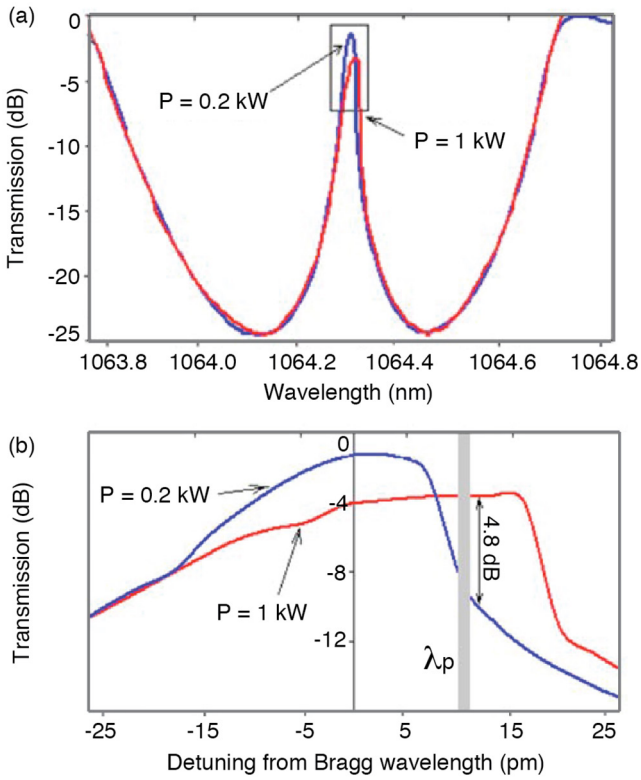

Figure 14. (a) Measured transmission of a π-shifted FBG versus wavelength for two different input powers. Adapted with permission from [19], The Optical Society, Copyright 2010. (b) Magnified version of (a) around the peaks showing a shift of 12 pm towards the longer wavelengths in the high power case (red) relative to the low power case (blue) and the non-Lorentzian shape of the peak.

When a high-power pulse (1 kW) was injected in the FBG, the leading edge of the output pulse became sharper (the rise time shortened) and the trailing edge extended further than the input pulse (the fall time increased). This happens because the nonlinear response of the grating is quite fast, making the leading edge steeper. On the other hand, when the switch is turned off the energy trapped inside the cavity escapes relatively slowly, leading to the observed extension of the trailing edge.

3.2.2. High intensity enhancement. Upham *et al* reported a much higher intensity enhancement in an apodized slow-light FBG [40]. The 1.2 cm Gaussian-apodized FBG, written with a femtosecond laser, exhibited several slow-light peaks in the transmission spectrum, from the short-wavelength edge of the grating to near the middle of the bandgap. The index profile of this grating, estimated by fitting its experimental transmission and reflection spectra via the transfer-matrix model, had a peak ac index modulation of 10^{-3}. The power loss coefficient, estimated in the same manner, was 0.057 dB cm^{-1} [40]. Using these parameters, the intensity enhancement as a function of position along the FBG was calculated for the six slow-light resonances closest to the bandgap (see figure 16). The black curves show the simulations for the actual FBG, taking into account its measured loss, while the red curves show the simulations for the same FBG assumed lossless. The intensity enhancement was maximum and equal to 800 for the third peak closest to the Bragg wavelength, and ~18

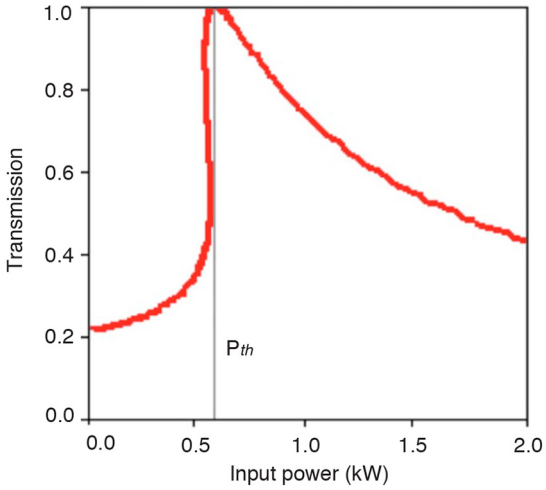

Figure 15. Normalized transmission of a π-shifted FBG versus input power for probe wavelength λ_p. Adapted with permission from [19], The Optical Society, Copyright 2010. The FBG is in the 'off' state for input powers lower than the threshold, and in the 'on' state for input powers higher than the threshold.

times larger than reported in the π-shifted FBG of [19]. For the same FBG with zero loss the predicted intensity enhancement is ~1.3 million. As demonstrated in earlier work on slow-light resonances [37], these results reaffirm the strong detrimental influence of FBG loss on the intensity enhancement. In addition, when sweeping a low-power (~0.3 mW) tunable laser across a slow-light peak, the intensity enhancement led to a shift in the peak's resonance wavelength and demonstrated peak broadening and bistability. Unlike in the π-shifted FBG of [19], however, this wavelength shift was not due to Kerr nonlinearity but due to heating of the FBG. Because of the high intensity circulating inside the FBG, optical power was converted to heat at a higher rate than in a normal fiber. This increased the FBG length (thermal expansion) and refractive index (thermo-optic effect) and shifted the resonance to higher wavelengths. A ~5 pm shift in the resonance was observed by applying an input power of less than 1 mW [40].

In [41], an intensity enhancement twice as large (1525) was reported in an apodized slow-light FBG. This enhancement was made possible by implementing three improvements to the grating design. The first two improvements were fabrication in a deuterium-loaded fiber and optimized annealing of the FBG in steps of 100 °C up to 300 °C for 30 min each. The general effects of these on the index modulation and loss, detailed in sections 2.3 and 3.1, facilitated the large intensity enhancement in the FBG.

The third improvement was the optimization of the FBG length for maximum intensity enhancement (see the calculated solid curves in figure 17(a)). To plot these curves, first, the experimental transmission and group delay spectra from a strong representative FBG were fitted to obtain the index profile shape and loss. The transfer matrix model was then used to compute the group delay and transmission of the fundamental mode of a grating with this profile shape and loss but with a length that was gradually increased from 1 mm to ~9 mm. For each length the mode volume and intensity enhancement were

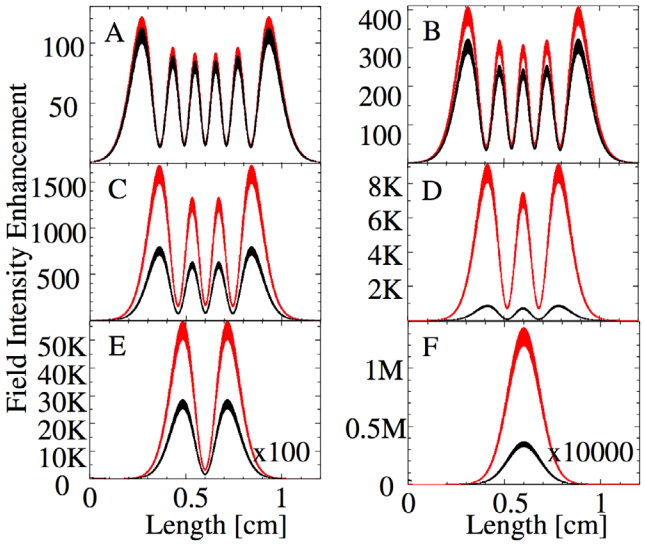

Figure 16. Calculated intensity enhancement for six peaks/modes (labeled (A)–(F) in increasing order of center wavelength) of a lossy (black) and a lossless (red) apodized FBG. Reprinted with permission from [40] The Optical Society, Copyright 2014.

computed by calculating the electric-field distribution along the FBG, as done for a stack of thin films [73]. These numerical calculations show (solid red curve in figure 17(a)) that as the FBG length is increased, the intensity enhancement first increases, because the reflectivity of the FBG increases and hence the group delay increases rapidly (for the same reason that the finesse of an FP increases when the reflectivity of the mirrors is increased), while the round-trip loss increases more slowly. When the length exceeds some value (~4 mm), the effect of the increasing propagation loss dominates and the intensity enhancement decreases. There is therefore an optimum FBG length for obtaining maximum intensity enhancement.

To verify these predictions, a ~4 mm FBG (close to optimum length) was fabricated, and its measured transmission spectrum was fitted to a model to infer the FBG's index profile and loss [41]. The narrowest resonance in the transmission spectrum had a measured Q factor of 7.3×10^6 after annealing and was experimentally verified to be the fundamental mode, the first such observation. Using these parameters the intensity enhancement dependence on length was then recalculated for these FBG parameters (dashed curve in figure 17(a)). As expected, the optimized length of the FBG maximized its intensity enhancement to 1525, the current record in an all-fiber device.

3.2.3. Large Purcell factors. The Purcell factor is a measure of the temporal and spatial confinement of light in a device. It is defined as [74]

$$F = \frac{3\lambda^3 Q}{4\pi^2 n^3 V_m} \tag{15}$$

where Q is the resonance quality factor and V_m is the mode volume. Achieving a high Purcell factor therefore requires a resonance with a high Q factor (equivalently, a large group delay) and a small mode volume. FBGs that combine short lengths with large group delays are therefore expected to exhibit high Purcell factors.

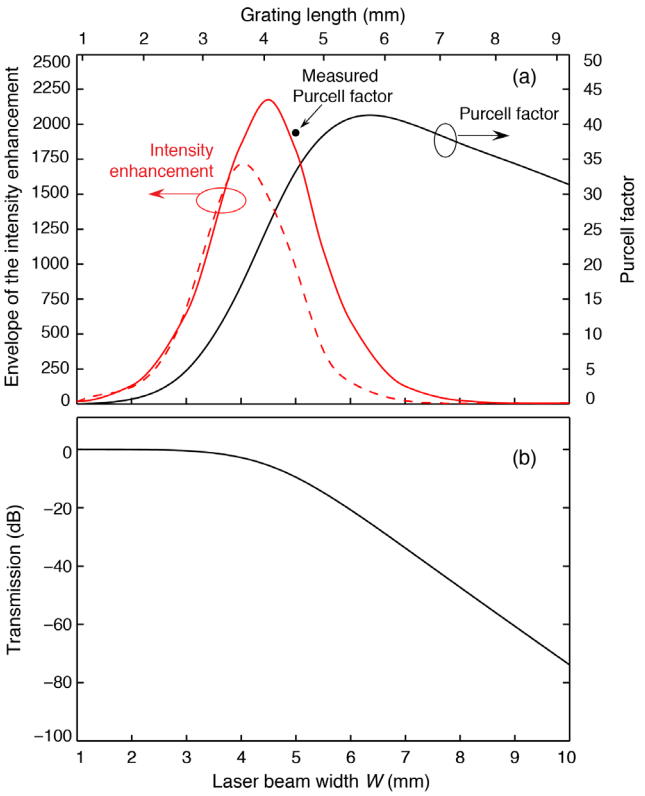

Figure 17. Simulated dependence on the laser beam width of (a) the intensity enhancement (red) for two FBGs (solid and dashed) and the Purcell factor (black) for an FBG (b) transmission at peak of slowest resonance versus grating length. Reprinted with permission from [41], The Optical Society, Copyright 2015.

In [41], a slow-light FBG with a Purcell factor of 38.7 was reported. To achieve this result, a length optimization similar to the one used to maximize the intensity enhancement (see section 3.2.2) was carried out to design an FBG with a maximum Purcell factor. Assuming an FBG with the known index-modulation profile shape and loss of a representative strong grating, the transfer matrix method was used to plot the transmission and group delay spectra of this FBG for increasing grating lengths. For each length, the Q factor of the fundamental mode was then calculated from the group delay, and the mode volume from the electric-field distribution, as described previously. Inserting these values in equation (15) gave the Purcell factor. The Purcell factor showed a similar theoretical dependence on length (solid black curve in figure 17(a)) as the intensity enhancement for the same physical reasons. The Purcell factor reached its maximum value (~41) for an optimum length of ~5.5 mm. The transmission at the peak of the slowest resonance, however, monotonically decreased with increase in FBG length (see figure 17(b)). As a compromise between high Purcell factor and high transmission, an FBG with a length of 4.5 mm was fabricated, slightly shorter than the optimum length. The FBG was annealed up to 250 °C to maximize the group delay and the Purcell factor. After annealing, the slowest resonance in the transmission spectra had a measured Q factor of 1.33×10^7 (group delay of 22 ns) and was experimentally verified to be the fundamental mode. The FBG's measured transmission and group delay spectra were fitted to obtain its index profile and loss. Using these

parameters, the mode volume was calculated to be 3.28×10^4 μm^3. These values gave a Purcell factor of 38.7 (filled circle in figure 17(a)), which is the largest Purcell factor reported in an all-fiber device.

Furthermore, the Q factor of the slow-light FBG with a group delay of 42 ns [26] (see section 3.1.1) was calculated to be ~3×10^7, one of the highest for a single-FBG device [25]. This Q factor is about twice as large as for the grating with the largest Purcell factor due to its lower loss (~0.2 m^{-1} versus ~0.44 m^{-1}).

The Purcell factor of 38.7 in [41] compares favorably to the Purcell factor of ~30 observed in a bitapered fiber FP placed between two FBGs [75]. This value resulted mostly from the very strong confinement afforded by the taper's 500 nm waist diameter. A high Purcell factor was also reported in a very short free-space FP resonator consisting of two high reflectors deposited on the curved tips of two single-mode fibers [76]. Placing the mirrors face to face close together formed a cavity with a mode waist radius of only ~1 μm, a high finesse of ~4×10^4, and a small mode volume of ~3 μm^3. The technology and care used during mirror machining and dielectric coating allowed the cavity finesse to be one order of magnitude greater [76] than reported before [77]. This cavity achieved a Purcell factor of 206 [76], which is of interest for applications in CQED, high-resolution optical filters, and gas spectroscopy, among others. In comparison, however, FBGs are smaller, significantly more robust, much easier to fabricate, and they require no alignment.

3.3. Sensors

3.3.1. Principle. Most FBG sensors are based on the same broad principle. When an external perturbation such as a longitudinal strain or a temperature change is applied to the grating, it modifies the period of the grating and the effective index of the fiber mode [78]. As a consequence, the Bragg wavelength (equation (13)) changes, causing the Bragg wavelength and the entire transmission (and reflection) spectrum of the grating to shift in the wavelength space [78]. This spectral shift is measured using one of many techniques, and the applied perturbation inferred from this measurement [79].

The method that has produced the highest resolution so far for strain sensing consists of measuring the shift with a laser. Light is launched into the FBG at a wavelength tuned to the steepest portion of the transmission (or reflection) spectrum of the grating (λ_{probe} in figure 18). The induced shift in the spectrum then results in the largest possible change in the power transmitted (or reflected) by the grating. The spectral shift can then be inferred from a simple measurement of this power change, and the applied perturbation recovered from the knowledge of the spectral shift.

The sensitivity of this class of sensor is defined as the change in the sensor output power dP_{out} divided by the small applied perturbation dx, normalized to the input power P_{in}:

$$S = \frac{1}{P_{in}}\left(\frac{dP_{out}}{dx}\right)_{\lambda_{probe}} = \left(\frac{dT}{dx}\right)_{\lambda_{probe}} = \left(\frac{dT}{d\lambda}\right)_{\lambda_{probe}} \frac{d\lambda_B}{dx} \qquad (16)$$

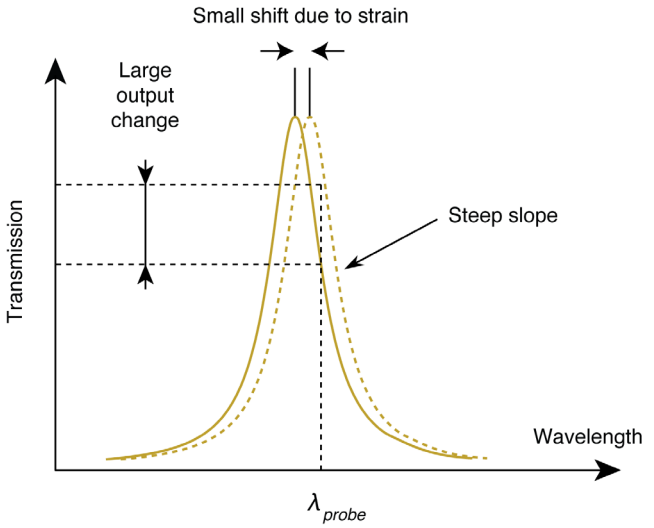

Figure 18. Sensing using a resonance. A small change in the FBG's environment causes the unperturbed slow-light peak (solid curve) to shift to a new position (dashed curve), and the transmission of the peak at the probe wavelength to change.

where $T = P_{out}/P_{in}$ is by definition the transmission of the FBG. The perturbation x can be the length, temperature, or acoustic pressure, among the most common examples. The second factor $d\lambda_B/dx$ describes the rate at which the Bragg wavelength (and the whole spectrum) shifts as a result of the application of a specific perturbation dx. For a given type of perturbation, this factor is a constant that depends in general only on the fiber material. For example, for strain sensing using an FBG fabricated in a silica fiber, $d\lambda_B/d\varepsilon = 0.78\lambda_B$, where ε is the applied strain [10]; for temperature sensing in the same type of fiber, $d\lambda_B/dT_0 = 8.08 \times 10^{-6}\ \lambda_B$ [10].

The first term in equation (16) is the slope of the peak at λ_{probe}. Equation (16) establishes the important result that the sensitivity is proportional to this slope, as expected: for a given spectral shift, a steeper slope yields a larger power change, and hence a larger sensitivity. A steep slope requires a narrow linewidth for the transmission peak, or equivalently a high quality factor or a large group delay. The strong slow-light resonances available either in the transmission resonance of a π-shifted grating (see figure 3), or on the edges of the bandgap in a strong FBG (see figure 5) are particularly beneficial for this general sensing scheme, because they can be significantly steeper than the band edges of a conventional FBG, and therefore they can provide significantly greater sensitivity. The connection between sensitivity and group delay can be easily derived analytically by considering the particular case of a resonance with a Lorentzian lineshape. It can then be shown easily that the maximum slope for a Lorentzian resonance is given by [63]:

$$\left(\frac{dT}{d\lambda}\right)_{\lambda_{probe},max} = 4c\frac{T_0\tau_g}{\lambda^2}, \qquad (17)$$

where T_0 is the peak transmission and τ_g the peak group delay of the resonance. Inserting this expression in equation (16) gives the maximum sensitivity for a Lorentzian slow-light resonance:

$$S_{\max} = 4c\frac{T_0\tau_g}{\lambda^2}\left(\frac{\mathrm{d}\lambda_B}{\mathrm{d}x}\right). \tag{18}$$

Importantly, the sensitivity is proportional to the group delay of the resonance (or the product of the group index by the length), and to its transmission. A higher group delay—slower light—leads to a steeper resonance slope, and therefore a higher sensitivity.

3.3.2. Noise sources and resolution. Mathematically, the minimum detectable perturbation $x_{\min}$ is the value of measurand x that gives a detected signal $\mathrm{d}P_{\mathrm{out}}$ equal to the output noise P_{noise}, or, using the first right hand side of equation (16) [63]:

$$S = \frac{1}{P_{\mathrm{in}}}\frac{P_{\mathrm{noise}}}{x_{\min}} \Rightarrow x_{\min} = \frac{1}{P_{\mathrm{in}}}\frac{P_{\mathrm{noise}}}{S}. \tag{19}$$

The minimum detectable signal (MDS) can then be interpreted as the noise expressed in units of measurand per root bandwidth, or equivalently the resolution of the sensor.

In slow-light FBG sensors, noise sources can be categorized in two general categories: sources that are independent of the sensor's sensitivity, and sources that depend on sensitivity. The first category includes the laser relative intensity noise (RIN), the photodetector noise, and shot noise (electrical and optical). The second category consists of the intrinsic thermodynamic phase noise of the fiber, the laser frequency noise, and environmental noise such as vibrations, acoustic noise, etc. Reference to equation (19) shows that the contribution to the MDS of any sensitivity-independent noise independent of sensitivity S can be reduced by increasing the sensitivity. When the sensitivity is high, the contribution from noise sources in the first category is negligible. On the other hand, noise sources in the second category being proportional to S, their contributions to the MDS (ratio of noise power to sensitivity, see equation (19)) are independent of sensitivity, and they cannot be reduced by increasing the sensitivity. Thus the limiting factor is noise sources of the second category. When this limit is reached, by increasing the sensitivity to render the first category negligible, further reduction in MDS can only be achieved by reducing the sensitivity-dependent noise contributions themselves.

3.3.3. Dynamic range. It is clear that sensitivity is only one of several important metrics in the characteristics of a sensor. The dynamic range, among others, is also a parameter that can be critical, although in general it does not vary from sensor to sensor by nearly as much as sensitivity. With reference to figure 18, the maximum detectable measurand is the measurand that needs to be applied to the FBG to shift its resonance peak to the probe wavelength. As the slope of the resonance is increased while maintaining the same peak transmission, the maximum detectable measurand obviously decreases, in proportion to the slope: the steeper the slope, the smaller the maximum detectable measurand. Both the minimum and the maximum detectable measurand are proportional to the slope. The dynamic range, which is the ratio of the two, is independent of the slope, or of the group delay of the resonance. This points to a tradeoff between minimum and maximum detectable measurand, an issue common to almost all optical sensors.

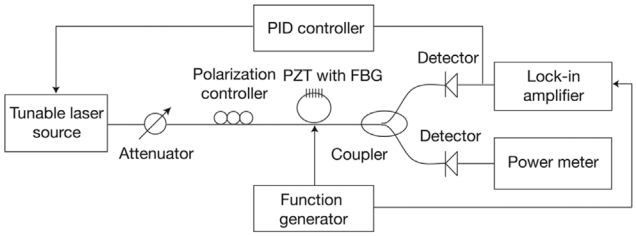

Figure 19. Experimental setup used to characterize the sensitivity and noise of the slow-light FBG strain sensor, and to stabilize its sensitivity against temperature variations (© [2013] IEEE. Reprinted, with permission, from [18]).

3.3.4. Strain sensors. One of the first uses of a sharp FBG resonance to demonstrate a strain sensor with a then-record resolution was reported in 2008 by Gatti *et al* [80], although at the time this type of resonance was not connected to slow light (which of course does not change the physics of the scheme). The resonance was the sharp transmission peak of a 3 cm π-shifted FBG. The sensor was interrogated as described in figure 19 with a laser with a broad linewidth (2 MHz), so that the noise was dominated by the laser frequency noise [80]. To cancel out environmental noise and drift (due to temperature fluctuations in particular), the Pound–Drevel–Hall (PDH) technique, which involves modulating the laser frequency and locking it to the maximum slope of the peak. Specifically, when the FBG's transmission peak shifted an error signal was applied to the laser frequency so that it tracked the peak. The error signal was proportional to the shift of the peak and therefore proportional to the applied strain too. Thus, the applied strain was measured by monitoring the error signal. This sensor had a measured MDS as low as 5 $\mathrm{p}\varepsilon\ (\sqrt{\mathrm{Hz}})^{-1}$ at frequencies above 100 kHz.

In 2012, this record was pushed back by more than one order of magnitude by using much slower light to increase the sensitivity, and by probing the FBG with a laser with much lower frequency noise [18]. The slow-light resonances were generated on the short-wavelength edge of a strong ($\Delta n_{\mathrm{ac}} \approx 10^{-3}$), slightly apodized grating 2 cm in length fabricated with a femtosecond laser at 403 nm. The slow-light peak used for sensing had a high transmission of 89%, corresponding to an internal grating loss of only 0.1 m^{-1}, one of the lowest reported for a grating this strong. The strain sensor was tested in the setup shown in figure 19. The light probe was an Agilent tunable laser with a narrow linewidth (8 kHz), which resulted in a very low laser frequency noise. A feedback system utilizing a simple PID controller was implemented to stabilize the sensor's sensitivity against low-frequency temperature fluctuations of the grating. Since the purpose of the feedback loop was to cancel only the drift, unlike in the PDH technique the laser frequency did not have to be modulated, which makes this scheme much simpler.

This sensor had a measured MDS of 280 $\mathrm{f}\varepsilon\ (\sqrt{\mathrm{Hz}})^{-1}$ at 23 kHz, limited also by laser frequency noise, the lowest strain resolution in a single FBG at the time of the publication [18].

The feedback circuit stabilized the sensitivity so well that the sensor output exhibited no sign of drift after continuous operation for 2 d. The absolute strain resolved by this sensor after integrating its output signal for ~6000 s was 200 fε.

This MDS record was improved by another order of magnitude in 2016 [81]. This ultra-low resolution was made possible mostly by reducing the laser frequency noise that was limiting the MDS in the previous sensor. This was accomplished by probing the sensor with a fiber laser from Orbits Lightwave that had a much narrower linewidth, namely under 200 Hz. Compared to the laser used for the previous sensor (linewidth of ~8 kHz), this new laser was expected to reduce the MDS by a factor of ~6 (assuming that the laser frequency noise scales as the square root of the linewidth, as it does in a semiconductor laser). The Orbits Lightwave laser was only slightly tunable. To maximize the number of FBGs that could be tested with this laser, we fabricated a large number of FBGs, and ordered a laser at the wavelengths that covered the largest number of FBGs. These gratings, including the one reported here, were fabricated with a longer-wavelength femtosecond laser (806 nm). They were also strongly apodized and thermally annealed. The 2 cm FBG reported here, after annealing up to 140 °C, had a slowest resonance with a group delay of ~11 ns and a peak transmission of ~55%. Based on these values, the expected sensitivity, proportional to the product Tn_gL [18], was ~1.8 times higher than the previous sensor. The MDS of this sensor probed on this slowest resonance was measured to be 120 fε $(\sqrt{\text{Hz}})^{-1}$ at 1 kHz and 30 fε $(\sqrt{\text{Hz}})^{-1}$ at 30 kHz. This last figure is the lowest reported for a fiber strain sensor.

To assess its long-term stability, this sensor was placed in an anechoic chamber (to reduce environmental noise), and its output was recorded for four continuous days, with no strain applied to it. The Allan variance calculated from this output trace is plotted in figure 20. Up to the maximum integration time shown in the figure (~8 h, or about 10% of the measurement duration), the sensor output exhibits no drift (variance slope of $-1/2$). The *absolute* strain resolved at the end of this 8 h integration (ordinate near the end point in the curve) is ~250 attostrains (2.5×10^{-16}), the lowest absolute strain ever reported for a fiber sensor.

3.3.5. Acoustic sensors. The exact same principle has also been used to measure weak acoustic pressures at sonic and ultrasonic frequencies. When an acoustic wave is incident on an FBG, two mechanisms take place [82]. First, the pressure strains the fiber radially at the acoustic frequency, which modulates the fiber refractive index. Second, due to the first principle of thermodynamics the surrounding temperature is also modulated, which modulates the temperature of the fiber, and thus its dimensions and refractive index. These two effects cause the Bragg wavelength and thus the whole reflection/transmission spectrum of the FBG to shift. Modeling shows that for a 125 μm diameter silica fiber, the thermal effect dominates below ~2 kHz, and the strain effect dominates above [82].

This principle was implemented in a π-shifted grating to demonstrate an ultrasonic sensor [83]. The grating was 2.38 mm long with a weak index modulation ($\Delta n_{ac} = 1.5 \times 10^{-5}$,

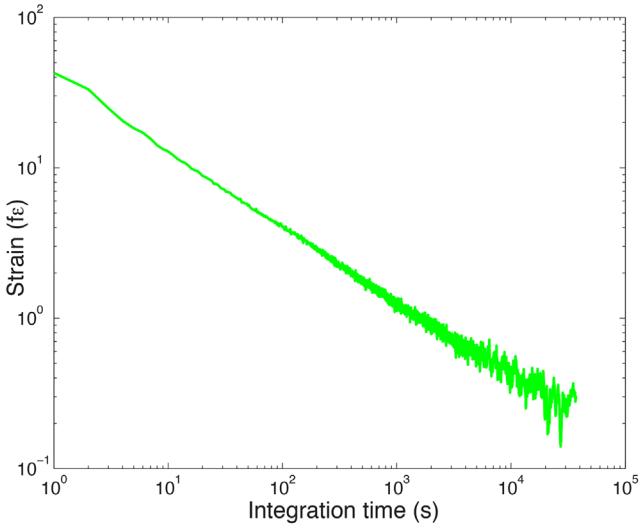

Figure 20. Measured Allan variance of the 30 fε $(\sqrt{\text{Hz}})^{-1}$ strain sensor showing an absolute strain resolution of ~250 attostrains after an integration time of ~8 h.

calculated from the coupling coefficient cited in [83]). The sensor's acoustic response was characterized by immersing the FBG in water 4.5 mm away from an underwater ultrasonic emitter. A calibrated needle microphone placed next to the FBG measured the pressure of the ultrasonic wave incident on the FBG. The laser frequency was tuned to the steepest slope of the FBG's transmission peak for maximum sensitivity. The lowest pressure that this sensor was able to detect at 10 MHz, inferred from a calibrated noise measurement, was 450 Pa. This high MDP was limited mainly by the relatively weak sensitivity of silica fibers to acoustic waves, and to a lower extent by the modest group index of the FBG resonance (its linewidth was 8 pm [83], corresponding to a group index of 40, calculated assuming a Lorentzian lineshape [63]).

To achieve a lower MDP, a mechanical transducer was used to convert the acoustic wave into a strain [84]. The transducer was a membrane attached normally to the fiber, as illustrated in figure 21. An acoustic wave incident on the membrane causes the latter to vibrate, and this vibration is transmitted to the fiber as a longitudinal strain at the acoustic frequency. The applied strain was measured using a π-shifted FBG. The measured minimum detectable pressure was 500 μPa $(\sqrt{\text{Hz}})^{-1}$ at 5 kHz.

A significantly better performance [81] was obtained by the authors of this article with a simpler design by using the strong slow-light FBG with an MDS of 30 fε $(\sqrt{\text{Hz}})^{-1}$ (see section 3.3.4). After annealing, the slow-light resonance with the steepest slope had a group delay of ~11 ns and a peak power transmission of ~55%. The MDP spectrum of this very simple sensor, measured in air in an anechoic chamber, had a flat band between roughly 500 Hz and 2 kHz, with an average value of 600 μPa $(\sqrt{\text{Hz}})^{-1}$ over this range. Between 3 kHz and 6 kHz the average MDP was as low as ~50 μPa $(\sqrt{\text{Hz}})^{-1}$. This value, which is about one order of magnitude lower than in [84], and which was achieved without resorting to a fragile membrane, further illustrates the exceptional performance attainable with slow-light gratings.

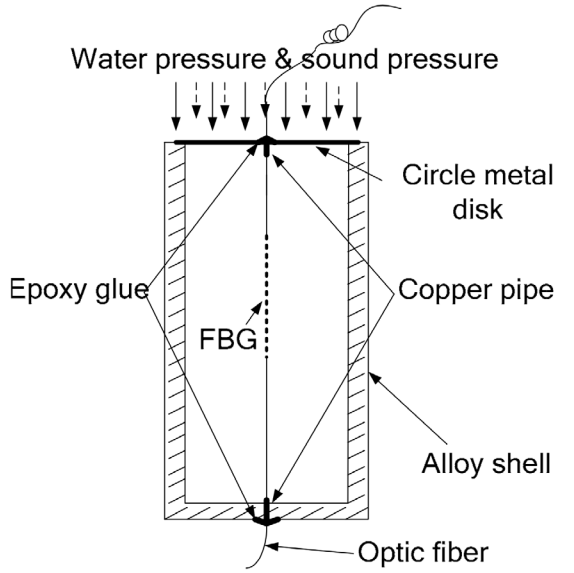

Figure 21. Transducer used in and reproduced from [84] under the Creative Commons Attribution License (CC BY), Springer, Copyright 2011. to convert an incident acoustic pressure to a strain.

4. Potential future applications and conclusion

Narrow slow-light resonances with high transmission can be formed in a low-loss FBG either with a strong apodized index-modulation profile or by introducing a phase shift in the middle of FBG. These resonances can exhibit very high group delays (up to 42 ns) and group indices (above 1000) in short gratings (1–2 cm). They have found demonstrated utility in communications (as filters to compute certain functions optically), as ultra-sensitive sensors (to detect in particular sub-picostrains and acoustic pressure), and in nonlinear optics (XPM, SPM, and optical switching). The recent demonstration in these devices of high Purcell factors also suggests interesting applications in quantum optics. Although a limited number of measurands have been investigated so far, it is clear that these sharp resonances can be applied to detect many other, in particular humidity, temperature, mechanical vibrations, and chemicals.

Further improvements in performance and in the already wide breadth of applications are expected in upcoming generations of FBGs by further reducing the internal loss, increasing the index modulation, optimizing the grating length and apodization profile, and better control of fluctuations in the index-modulation period, phase, and amplitude during fabrication. Similar advancements are anticipated to benefit π-shifted fiber Bragg gratings as well.

Acknowledgment

The portion of the work reported herein that was carried out at Stanford University was supported by Northrop Grumman Corporation. The portion of the research performed at Laval University was supported by the Natural Science and Engineering Research Council of Canada and the Canada Foundation for Innovation.

References

[1] Meltz G, Morey W W and Glenn W H 1989 Formation of Bragg gratings in optical fibers by a transverse holographic method *Opt. Lett.* **14** 823–5
[2] Bernier M, Sheng Y and Vallée R 2009 Ultrabroadband fiber Bragg gratings written with a highly chirped phase mask and infrared femtosecond pulses *Opt. Express* **17** 3285–90
[3] Archambault J L, Reekie L and Russell P J 1993 High reflectivity and narrow bandwidth fibre gratings written by single excimer pulse *Electron. Lett.* **29** 28–9
[4] Archambault J L, Reekie L and Russell P S J 1993 100% reflectivity Bragg reflectors produced in optical fibres by single excimer laser pulses *Electron. Lett.* **29** 453–5
[5] Lemaire P J, Vengsarkar A M, Reed W A, Mizrahi V and Kranz K S 1994 Refractive index changes in optical fibers sensitized with molecular hydrogen *Conf. on Optical Fiber Communication, OSA Technical Digest Series* vol 4 (Optical Society of America) pp 47–8
[6] Hill K O, Fujii Y, Johnson D C and Kawasaki B S 1978 Photosensitivity in optical fiber waveguides: application to reflection filter fabrication *Appl. Phys. Lett.* **32** 647–9
[7] Agrawal G P and Radic S 1994 Phase-shifted fiber Bragg gratings and their application for wavelength demultiplexing *IEEE Photon. Technol. Lett.* **6** 995–7
[8] Ball G A and Glenn W H 1992 Design of a single-mode linear-cavity erbium fiber laser utilizing Bragg reflectors *J. Lightwave Technol.* **10** 1338–43
[9] Lord S M, Switzer G W and Krainak M A 1996 Using fibre gratings to stabilise laser diode wavelength under modulation for atmospheric lidar transmitters *Electron. Lett.* **32** 561–3
[10] Kersey A D, Davis M A, Patrick H J, LeBlanc M, Koo K P, Askins C G, Putnam M A and Friebele E J 1997 Fiber grating sensors *J. Lightwave Technol.* **15** 1442–63
[11] Othonos A and Kalli K 1999 *Fiber Bragg Gratings Fundamentals and Applications in Telecommunications and Sensing* (Boston, MA: Artech House Publishers) pp 301–89
[12] Erdogan T 1997 Fiber grating spectra *J. Lightwave Technol.* **15** 1277–94
[13] Sipe J E, Poladian L and De Sterke C M 1994 Propagation through nonuniform grating structures *J. Opt. Soc. Am.* A **11** 1307–20
[14] Gehring G M, Boyd R W, Gaeta A L, Gauthier D J and Willner A E 2008 Fiber-based slow-light technologies *J. Lightwave Technol.* **26** 3752–62
[15] Matsuhara M and Hill K O 1974 Optical-waveguide band-rejection filters: design *Appl. Opt.* **13** 2886–8
[16] Cross P S and Kogelnik H 1977 Sidelobe suppression in corrugated-waveguide filters *Opt. Lett.* **1** 43–5
[17] Albert J, Hill K O, Malo B, Thériault S, Bilodeau F, Johnson D C and Erickson L E 1995 Apodization of the spectral response of fiber Bragg gratings using a phase mask with variable diffraction efficiency *Electron. Lett.* **31** 222–3
[18] Wen H, Skolianos G, Fan S, Bernier M, Vallée R and Digonnet M J 2013 Slow-light fiber-Bragg-grating strain sensor with a 280 femtostrain $(\sqrt{\text{Hz}})^{-1}$ resolution *J. Lightwave Technol.* **31** 1804–8
[19] Kabakova I V, De Sterke C M and Eggleton B J 2010 Bistable switching and reshaping of optical pulses in a Bragg grating cavity *J. Opt. Soc. Am.* B **27** 2648–53
[20] Melloni A, Chinello M and Martinelli M 2000 All-optical switching in phase-shifted fiber Bragg grating *IEEE Photon. Technol. Lett.* **12** 42–4
[21] Baba T and Sano D 2003 Low-threshold lasing and Purcell effect in microdisk lasers at room temperature *IEEE J. Sel. Top. Quantum Electron.* **9** 1340–6

[22] Vernooy D, Ilchenko V, Mabuchi H, Streed E and Kimble H 1998 High-*Q* measurements of fused-silica microspheres in the near infrared *Opt. Lett.* **23** 247–9

[23] Margolis H S, Edwards C S, Barwood G P and Gill P 2002 A passive optical frequency comb for frequency metrology in the 1.5 micron optical communications band *Lasers Electro-Optics Society, 2002 The 15th Annual Meeting of the IEEE* vol 1 pp 229–30

[24] Kippenberg T J, Spillane S M and Vahala K J 2004 Demonstration of ultra-high-*Q* small mode volume toroid microcavities on a chip *Appl. Phys. Lett.* **85** 6113–5

[25] Skolianos G, Arora A, Bernier M and Digonnet M J 2015 Slowing down light to 300 km s^{-1} in a deuterium-loaded fiber Bragg grating *Opt. Lett.* **40** 1524–7

[26] Kashyap R 2010 *Fiber Bragg Gratings* 2nd edn (New York: Academic) p 142

[27] Eggleton B J, Stephens T, Krug P A, Dhosi G, Brodzeli Z and Ouellette F 1996 Dispersion compensation using a fibre grating in transmission *Electron. Lett.* **32** 1610–1

[28] Agrawal G P 2010 *Fiber-Optic Communications Systems* 4th edn (New York: Wiley) p 356

[29] Dong L, Cole M J, Ellis A D, Laming R I and Widdowson T 1997 40 Gbit s^{-1} 1.55 μm RZ transmission over 109 km of non-dispersion shifted fibre with long continuously chirped fibre gratings *Electron. Lett.* **33** 1563–5

[30] Longhi S 2005 Group delay tuning in active fiber Bragg gratings: from superluminal to subluminal pulse reflection *Phys. Rev.* E **72** 056614

[31] Longhi S, Janner D, Galzerano G, Valle G D, Gatti D and Laporta P 2005 Optical buffering in phase-shifted fiber gratings *Electron. Lett.* **41** 1075–6

[32] Longhi S, Marano M, Laporta P, and Belmonte M 2001 Superluminal optical pulse propagation at 1.5 μm in periodic fiber Bragg gratings *Phys. Rev.* E **64** 055602

[33] Janner D, Galzerano G, Valle G D, Laporta P, Longhi S and Belmonte M 2005 Slow light in periodic superstructure Bragg gratings *Phys. Rev.* E **72** 056605

[34] Pisco M, Ricciardi A, Campopiano S, Caucheteur C, Mégret P, Cutolo A and Cusano A 2009 Fast and slow light in optical fibers through tilted fiber Bragg gratings *Opt. Express* **17** 23502–10

[35] Gagné M, Loranger S, Lapointe J and Kashyap R 2014 Fabrication of high quality, ultra-long fiber Bragg gratings: up to 2 million periods in phase *Opt. Express* **22** 387–98

[36] Qian K, Zhan L, Li H, Hu X, Peng J, Zhang L and Xia Y 2009 Tunable delay slow-light in an active fiber Bragg grating *Opt. Express* **17** 22217–22

[37] Wen H, Skolianos G, Fan S and Digonnet M J 2011 Slow light in fiber Bragg gratings *Proc. SPIE 7949 Advances in Slow and Fast Light IV (17 February 2011)* p 79490E

[38] Wen H, Terrel M, Fan S and Digonnet M J 2012 Sensing with slow light in fiber Bragg gratings *IEEE Sens. J.* **12** 156–63

[39] Siegman A 1986 *Lasers* (Mill Valley, CA: University Science Books) pp 413–27

[40] Upham J, Leon I D, Grobnic D, Ma E, Dicaire M N, Schulz S A, Murugkar S and Boyd R W 2014 Enhancing optical field intensities in Gaussian-profile fiber Bragg gratings *Opt. Lett.* **39** 849–52

[41] Skolianos G, Arora A, Bernier M and Digonnet M J 2015 High Purcell factor in fiber Bragg gratings utilizing the fundamental slow-light mode *Opt. Lett.* **40** 3440–3

[42] Skolianos G, Arora A, Bernier M and Digonnet M J 2015 Strong slow-light resonances in apodized deuterium-loaded femtosecond FBGs *Proc. SPIE 9378, Slow Light, Fast Light, and Opto-Atomic Precision Metrology VIII (10 March 2015)* p 93780E

[43] Skolianos G, Bernier M, Vallée R and Digonnet M J 2014 Observation of ~20 ns group delay in a low-loss apodized fiber Bragg grating *Opt. Lett.* **39** 3978–81

[44] Kashyap R 2010 *Fiber Bragg Gratings* 2nd edn (New York: Academic) pp 35–7

[45] Hand D P and Russell P S 1990 Photoinduced refractive-index changes in germanosilicate fibers *Opt. Lett.* **15** 102–4

[46] Othonos A and Kalli K 1999 *Fiber Bragg Gratings Fundamentals and Applications in Telecommunications and Sensing* (Boston, MA: Artech House Publishers) p 25

[47] Gusarov A I and Doyle D B 2000 Contribution of photoinduced densification to refractive-index modulation in Bragg gratings written in Ge-doped silica fibers *Opt. Lett.* **25** 872–4

[48] Limberger H G, Fonjallaz P Y, Salathé R P and Cochet F 1996 Compaction- and photoelastic-induced index changes in fiber Bragg gratings *Appl. Phys. Lett.* **68** 3069–71

[49] Fonjallaz P Y, Cochet F, Leuenberger B, Limberger H G and Salathé R P 1995 Tension increase correlated to refractive-index change in fibers containing UV-written Bragg gratings *Opt. Lett.* **20** 1346–8

[50] Tsai T E, Williams G M and Friebele E J 1997 Index structure of fiber Bragg gratings in Ge–SiO_2 fibers *Opt. Lett.* **22** 224–6

[51] Atkins R M and Lemaire P J 1992 Effects of elevated temperature hydrogen exposure on short-wavelength optical losses and defect concentrations in germanosilicate fibers *J. Appl. Phys.* **72** 344–8

[52] Stone J 1987 Interactions of hydrogen and deuterium with silica optical fibers: a review *J. Lightwave Technol.* **5** 712–33

[53] Bernier M, Gagnon S and Vallée R 2011 Role of the 1D optical filamentation process in the writing of first order fiber Bragg gratings with femtosecond pulses at 800 nm (Invited) *Opt. Mater. Express* **1** 832–44

[54] Mihailov S J, Smelser C W, Lu P, Walker R B, Grobnic D, Ding H, Henderson G and Unruh J 2003 Fiber Bragg gratings made with a phase mask and 800 nm femtosecond radiation *Opt. Lett.* **28** 995–7

[55] Smelser C W, Mihailo S J and Grobnic D 2005 Formation of Type I-IR and Type II-IR gratings with an ultrafast IR laser and a phase mask *Opt. Express* **13** 5377–86

[56] Martinez A, Dubov M, Khrushchev I and Bennion I 2004 Direct writing of fibre Bragg gratings by femtosecond laser *Electron. Lett.* **40** 1170–2

[57] Malo B, Theriault S, Johnson D C, Bilodeau F, Albert J and Hill K O 1995 Apodised in-fibre Bragg grating reflectors photoimprinted using a phase mask *Electron. Lett.* **31** 223–4

[58] Singh H and Zippin M 1998 Apodized fiber Bragg gratings for DWDM applications using uniform phase mask in *Proc. of the 24th European Conf. on Optical Communication (Lerko Print S.A., Madrid, 1998)* vol 1 pp 189–90

[59] Martin J, Lauzon J, Thibault S and Ouellette F 1994 Novel writing technique of long highly reflective in fiber gratings and investigation of the linearly chirped component *Post-Deadline Paper PD29-1, Proc. Conf. on Optical Fiber Communications, OFC'94* p 138

[60] Loh W H, Cole M J, Zervas M N, Barcelos S and Laming R I 1995 Complex grating structures with uniform phase masks based on the moving fiber-scanning beam technique *Opt. Lett.* **20** 2051–3

[61] Bernier M, Trépanier F, Carrier J and Vallée R 2014 High mechanical strength fiber Bragg gratings made with infrared femtosecond pulses and a phase mask *Opt. Lett.* **39** 3646–9

[62] Bernier M, Vallée R, Morasse B, Desrosiers C, Saliminia A and Sheng Y 2009 Ytterbium fiber laser based on first-order fiber Bragg gratings written with 400 nm femtosecond pulses and a phase-mask *Opt. Express* **17** 18887–93

[63] Wen H 2012 Ultra-high sensitivity strain sensor using slow light in fiber Bragg gratings *PhD Dissertation* Stanford University

[64] Meltz G and Morey W W 1991 Bragg grating formation and germanosilicate fiber photosensitivity *Proc. SPIE 1516, Int. Workshop on Photoinduced Self-Organization Effects in Optical Fiber (30 December 1991)* pp 185–99
[65] Martinez A, Khrushchev I Y and Bennion I 2005 Thermal properties of fibre Bragg gratings inscribed point-by-point by infrared femtosecond laser *Electron. Lett.* **41** 176–8
[66] Berger N K, Levit B, Fischer B, Kulishov M, Plant D V and Azaña J 2006 All-optical temporal differentiator based on a single phase-shifted fiber Bragg grating *Lasers and Electro-Optics Society 2006, 19th Annual Meeting of the IEEE* pp 370–71
[67] Curatu G, LaRochelle S, Pare C and Belanger P A 2001 Pulse shaping with a phase-shifted fiber Bragg grating for antisymmetric pulse generation *Proc. SPIE 4271, Optical Pulse and Beam Propagation III (12 April 2001)* pp 213–21
[68] Mok J T, de Sterke C M and Eggleton B J 2006 Delay-tunable gap-soliton-based slow-light system *Opt. Express* **14** 11987–96
[69] Ge J, Wang C and Zhu X 2010 Optical Hilbert transform using fiber Bragg gratings *Proc. SPIE 7851, Information Optics and Optical Data Storage (2 December 2010)* p 785117
[70] Zhang C, Ning T, Li C, Jian W, Chen H, Yan L and Zheng J 2013 Application of phase-shifted fiber Bragg grating in single sideband transmission–based radio-over-fiber system *Opt. Eng.* **52** 115101
[71] Bravo-Abad J, Rodriguez A, Bermel P, Johnson S, Joannopoulos J D and Soljacic M 2007 Enhanced nonlinear optics in photonic-crystal microcavities *Opt. Express* **15** 16161–76
[72] Agrawal G P 2010 *Fiber-Optic Communications Systems* 4th edn (New York: Wiley) p 64
[73] Troparevsky M C, Sabau A S, Lupini A R and Zhang Z 2010 Transfer-matrix formalism for the calculation of optical response in multilayer systems: from coherent to incoherent interference *Opt. Express* **18** 24715–21
[74] Purcell E M 1946 Spontaneous emission probabilities at radio frequencies *Phys. Rev.* **69** 681
[75] Wuttke C, Becker M, Bruckner S, Rothhardt M and Rauschenbeutel A 2012 Nanofiber Fabry–Perot microresonator for nonlinear optics and cavity quantum electrodynamics *Opt. Lett.* **37** 1949–51
[76] Hunger D, Steinmetz T, Colombe Y, Deutsch C, Hänsch T W and Reichel J 2010 A fiber Fabry–Perot cavity with high finesse *New J. Phys.* **12** 065038
[77] Steinmetz T, Colombe Y, Hunger D, Hänsch T W, Balocchi A, Warburton R J and Reichel J 2006 Stable fiber-based Fabry–Pérot cavity *Appl. Phys. Lett.* **89** 111110
[78] Rao Y J 1997 In-fibre Bragg grating sensors *Meas. Sci. Technol.* **8** 355–75
[79] Zhao Y and Liao Y 2004 Discrimination methods and demodulation techniques for fiber Bragg grating sensors *Opt. Lasers Eng.* **41** 1–18
[80] Gatti D, Galzerano G, Janner D, Longhi S and Laporta P 2008 Fiber strain sensor based on a π-phase-shifted Bragg grating and the Pound–Drever–Hall technique *Opt. Express* **16** 1945–50
[81] Digonnet M, Skolianos G and Arora A 2016 Measuring attostrains in a slow-light fiber Bragg grating *Invited Paper in SPIE: Slow Light, Fast Light, and Opto-Atomic Precision Metrology IX (San Francisco, 17 February 2016)* (doi: 10.1117/12.2220219)
[82] Løvseth S W, Kringlebotn J T, Rønnekleiv E and Bløtekjær K 1999 Fiber distributed-feedback lasers used as acoustic sensors in air *Appl. Opt.* **38** 4821–30
[83] Rosenthal A, Razansky D and Ntziachristos V 2011 High-sensitivity compact ultrasonic detector based on a pi-phase-shifted fiber Bragg grating *Opt. Lett.* **36** 1833–5
[84] Huang S, Jin X, Zhang J, Chen Y, Wang Y, Zhou Z and Ni J 2011 An optical fiber hydrophone using equivalent phase shift fiber Bragg grating for underwater acoustic measurement *Photonic Sensors* **1** 289–94